

---

# Multibeam Laser–Plasma Interactions in Inertial Confinement Fusion

## Introduction

Of the many challenges facing laser-driven inertial confinement fusion (ICF),<sup>1,2</sup> controlling the impact of laser–plasma interactions (LPI’s) is one of the most difficult and uncertain.<sup>3</sup> The importance of LPI’s in indirect-drive–ignition experiments at the National Ignition Facility (NIF) is now widely appreciated because of the dramatic impact of instabilities on the capsule implosion symmetry.<sup>4,5</sup> Perhaps less well known are the effects in the alternative direct-drive approach.<sup>6</sup> This article highlights some of the discoveries and recent advances in understanding these instabilities—the most important of which is the realization that the collective interaction of multiple beams is ubiquitous throughout laser fusion.

It is important to understand the instabilities resulting from intense LPI’s in ICF because they place bounds on the available ignition regimes/design space. For example, higher radiation temperatures in indirect drive or higher ablation pressures in direct drive, minimize hydrodynamic instabilities and improve target performance, but they require higher laser intensities, which are more vulnerable to instability.<sup>7</sup> Instabilities involving the cooperation between multiple laser beams are particularly dangerous because their onset can occur at intensities significantly below that of non-cooperative, i.e., single-beam, interactions. The mitigation of multibeam instabilities is therefore of great importance to the success of ICF.

Laser–plasma instabilities are fundamentally difficult to understand and predict because they involve a severe coupling of spatial and temporal scales. Large-scale plasma hydrodynamics are evolved with radiation–hydrodynamics codes (e.g., *LASNEX*<sup>8</sup> or *DRACO*<sup>9</sup>) over spatial regions that are millimeters in extent and over times that span tens of nanoseconds. On the other hand, LPI’s involve the coherent interaction between waves that have high characteristic frequencies ( $\sim 10^{15}$  s<sup>-1</sup>) and short wavelengths ( $\sim 0.1$   $\mu$ m). The plasma conditions and laser irradiation determine the conditions under which LPI’s can grow,<sup>10</sup> but the instabilities, in turn, modify the hydrodynamics by redirecting the laser light,<sup>11</sup> modifying absorption, or producing hot electrons. The only practical approach to

addressing these problems is by developing simplified models that can be run self-consistently in the hydrodynamics codes (for examples of such “in-line” models, see **SBS-Mediated CBET in ICF Experiments**, p. 63).

The difficulties of multiple scales exist even in numerical models of LPI’s that do not attempt to describe large-scale hydrodynamic evolution. Explicit particle-in-cell (PIC) codes,<sup>12,13</sup> such as *OSIRIS*<sup>14</sup> and *VPIC*,<sup>15</sup> are highly detailed plasma-kinetic models that make few simplifying assumptions regarding the plasma response; however, they are too expensive to run in three dimensions for scale lengths and times of relevance for ignition conditions (the advent of petascale computing may change this in the future). These problems have been partially addressed by the development of reduced models that exploit temporal and/or spatial enveloping (multiple scales)<sup>16</sup> and either ignore the particle kinetics (i.e., plasma-fluid codes) or treat the kinetics in a simplified way (e.g., the codes *pF3D*,<sup>17</sup> *Harmony*,<sup>18</sup> and *ZAK3D*.<sup>19,20</sup> Several examples of the application of these models will be described in this article.

The above comments apply to single-beam interactions as well as to situations involving the cooperative interaction between multiple laser beams. The importance of multibeam interactions places a much-greater emphasis on the three-dimensional (3-D) geometry than before and requires numerical simulations to be more “realistic.” This article will review recent advances in this regard.

The following sections (1) introduce LPI’s in laser fusion, describing the two major approaches and discussing the similarities and differences with respect to LPI conditions; (2) describe three-wave parametric instabilities, focusing on the interaction of instabilities occurring in different beams; (3) introduce cross-beam energy transfer (CBET), describing the effect and reviewing the experimental impact in both direct- and indirect-drive experiments; (4) describe multibeam stimulated Raman scattering and two-plasmon decay; (5) describe strategies that have been designed to mitigate multibeam instabilities; and, finally, (6) present our summary and conclusions.

## Two Approaches to Laser Fusion at the National Ignition Facility

There are two primary approaches to laser-driven ICF: indirect drive, where the laser energy is first converted to x rays in a hohlraum (Fig. 137.48) that subsequently drives the target,<sup>21</sup> and direct drive, where the laser light deposits its energy directly onto the capsule (Fig. 137.49).

A major effort<sup>22,23</sup> is underway to demonstrate indirect-drive ignition on the NIF.<sup>24</sup> Since the NIF beamlines are not configured for spherically symmetric direct drive, LLE has developed the polar-drive (PD) concept.<sup>25</sup> This concept makes it possible to explore direct-drive ignition on the NIF while the beamlines are in the indirect-drive configuration.

LLE's Omega Laser Facility<sup>26–28</sup> performs direct-drive ICF research in both the favored spherically symmetric and polar-drive configurations at relatively modest driver energies with the goal of validating designs that, when scaled to the NIF, would show ignition and gain (i.e., hydro-equivalent designs).<sup>29</sup> Recent progress has led to a series of PD designs that are predicted to marginally ignite on the NIF,<sup>30</sup> provided LPI's at the NIF scale do not present new challenges.

### 1. Indirect Drive

The NIF is currently configured for the polar illumination that is required for indirect-drive experiments. The individual 192 beams are clustered into groups of four (called quadruplets, or “quads”) that share a common entrance port on the target chamber. At each pole of the target chamber the quads are grouped into two cones. There are eight quads in each inner cone and 16 in the outer cones. With this arrangement one-third of the laser energy is in the inner cones that preferentially drive the waist (or equator) of the capsule, while the remaining two-thirds of the energy preferentially drives the polar regions of the indirect-drive target/capsule. Figure 137.48 shows this arrangement, together with the specific beam angles.

The cylindrical NIF hohlraum (Fig. 137.48) is ~10 mm long and slightly more than 5 mm in diameter. The laser beams enter through two laser entrance holes (LEH's), one at each end, propagate through the gas-filled interior, and deposit their energy at the high-Z hohlraum walls, generating soft x-ray radiation. These x rays drive the implosion of the capsule that is suspended in the hohlraum. By design, the beam pointing and dynamically varying relative power between the two cones of beams are chosen so that the x-ray drive, as seen by the cap-

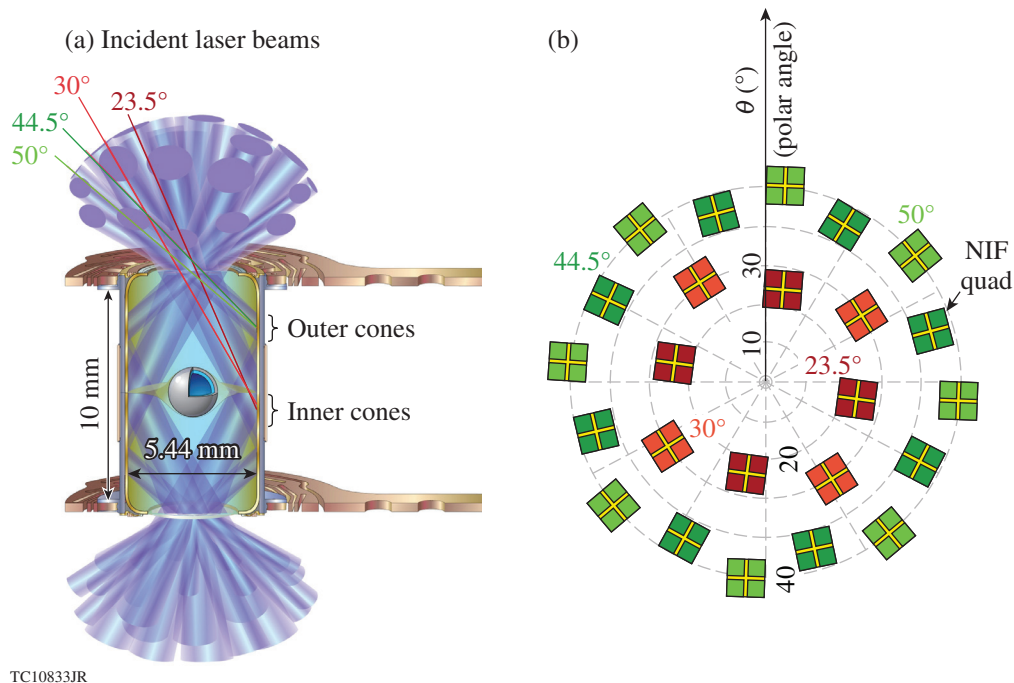


Figure 137.48

(a) A schematic of a NIF ignition hohlraum with the approximate dimensions, showing the inner and outer beam cones entering the hohlraum through the two laser entrance holes. (b) The specific angles of the NIF beam quads, which are color coded: inner quads orange ( $\theta = 30^\circ$ ) and red ( $\theta = 23.5^\circ$ ), and outer quads light ( $\theta = 50^\circ$ ) and dark green ( $\theta = 44.5^\circ$ ), where  $\theta$  is the polar angle.

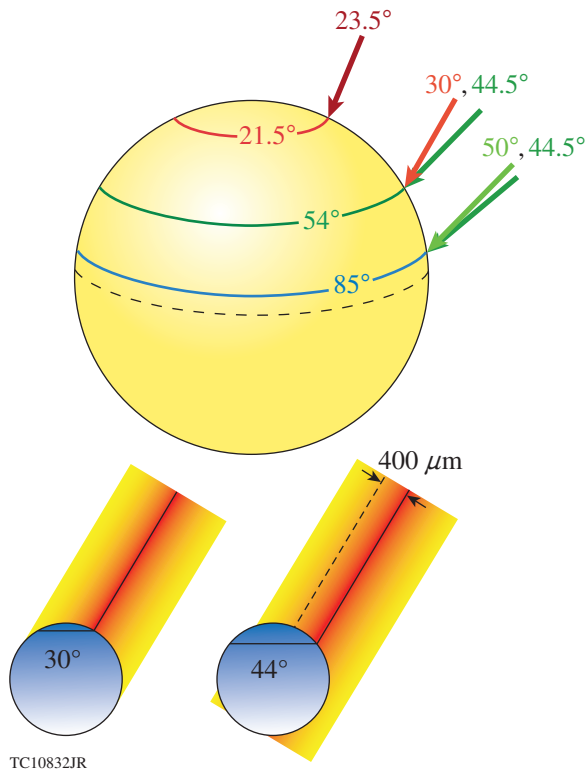


Figure 137.49  
 Polar drive on the NIF is achieved by repointing the NIF beams to compensate for the lack of beams at the equator (Fig. 137.48). The repointing is greatest for beams in the outer cone (having angles of 44.5° and 50°) to provide sufficient drive on the equator of the target (dashed line).

sule, is uniform (to within 1% time averaged).<sup>31</sup> The cryogenic ignition hohlraum is filled with a low-density helium gas fill that is quickly ionized and becomes a high-temperature, low-density plasma. Its purpose is to retard the inward expansion of the gold hohlraum walls as they are heated.

As will be described in **Cross-Beam Energy Transfer** (p. 63), the frequencies (or, equivalently, the wavelengths) of the NIF quads may be shifted with respect to one another. The two-color separation on the NIF consists of shifting the wavelength of the outer cone of beams with respect to that of the inner cones by  $\sim \Delta\lambda = 0$  to  $8 \text{ \AA}$  (at  $1\omega_0$ ). A three-color option also exists, where there are two tunable wavelength separations: (1) the separation between the frequency of the outer cones and the inner 30° quads; and (2) the separation between the inner 30° quad and the inner 23.5° quad.<sup>11,32</sup>

## 2. Polar Drive

The NIF was designed so that an option remains for imploding spherically symmetric direct-drive-ignition targets.<sup>31</sup> In direct drive, the laser beams illuminate and implode the

target directly without the intermediate step of converting to x rays. As a result, direct drive is predicted to couple  $7\times$  to  $9\times$  more energy to the compressed capsule than indirect drive.<sup>33</sup> Because reconfiguration of the NIF beam architecture is very invasive, the PD scheme was conceived so that directly driven experiments can be performed while the NIF remains in the indirect-drive configuration.<sup>25</sup>

Polar-drive-ignition designs rely on repointing the NIF beams (Fig. 137.48) toward the equator of the target (Fig. 137.49) by using different pulse shapes for different rings of the NIF configuration and using specialized phase plates to achieve sufficient implosion symmetry in the absence of equatorial beams. Accurate modeling of oblique-beam energy deposition, the effect of beam obliquity on LPI's in the underdense corona, and heat transport to the ablation surface are critical to achieving sufficient symmetry, implosion velocity, and shell adiabat.<sup>6,30</sup>

## 3. Comparison of LPI Between Indirect-Drive and Polar-Drive Schemes

Figure 137.50(a) shows a contour plot of the coronal electron plasma density (normalized to the critical density) for an ignition-scale direct-drive target, with the approximate dimensions indicated. Sample ray trajectories, approximately corresponding to three cones of beams, are overlaid. For comparison, a NIF-scale indirect-drive hohlraum is shown in Fig. 137.50(b). Again, the electron plasma density is shown with the laser-beam trajectories overlaid. The two figures are not shown on the same scale.

The plasma conditions differ quite significantly between the two cases. The plasma density scale length for the direct-drive target is  $L_n \sim 500$  to  $600 \mu\text{m}$  (the density decreasing with radius  $r$ ), the coronal electron temperature is approximately isothermal with  $T_e = 3$  to  $4 \text{ keV}$ , and the baseline design uses a CH ablator. The plasma-flow velocity is directed radially outward, increasing with radius. The Mach-1 surface is located at a radius where the electron plasma density  $n_e$  is approximately one quarter of the critical density  $n_e(r) \approx n_c/4$  (the quarter-critical surface), where  $n_c = m_e \omega_0^2 / (4\pi e^2)$  is the density at which electromagnetic (EM) waves of frequency  $\omega_0$  are reflected (see Fig. 137.50).<sup>3</sup> The quantities  $e$  and  $m_e$  are the electron charge and mass, respectively. This is to be contrasted with the indirect-drive hohlraum. The plasma density inside the hohlraum is more homogeneous ( $L_n \sim \text{mm}$ 's) and the plasma flow structure is quite complicated, with the Mach-1 surface falling just outside the LEH's. [The LEH has been shown to act like a sonic nozzle (in analogy with gas dynamics) so the flow external to the nozzle is quite insensitive to changes within the

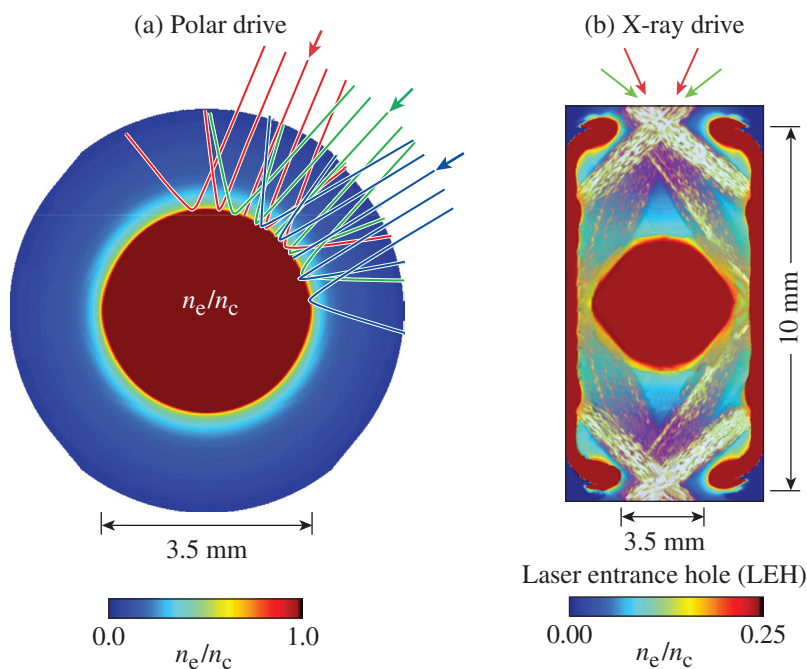


Figure 137.50

(a) In direct-drive targets, multiple laser beams overlap everywhere in the underdense corona over a wide range of angles (rays corresponding to three representative beams are shown). (b) In indirect-drive targets, multiple beams overlap in the neighborhood of the laser entrance holes with a limited number of angles. The color bars indicate the electron plasma density normalized to the critical density (note the different density scales on the left and right).

hohlraum.<sup>34]</sup> The electron temperature is  $T_e = 2$  to 4 keV and is highest in the beam-overlap region near the LEH. The laser light interacts with a mixture of different materials: the He (or He/H) gas that fills the hohlraum, Au plasma ablated from the hohlraum walls, and CH plasma ablated from the target.

The laser-beam intensities are quite different between the two schemes. In indirect drive, the single-beam intensities are nominally  $1 \times 10^{15}$  W/cm<sup>2</sup> for the outer cone quads and  $0.5 \times 10^{15}$  for the inner cone at the LEH, while in direct drive, the single-beam intensities are lower:  $\sim 1 \times 10^{14}$  W/cm<sup>2</sup>. The differences in laser intensity are determined by design considerations. In indirect drive, the LEH's through which the beams propagate must be as small as possible since the area of the LEH is a sink for x rays. This requires small beam spots and high beam intensities. In direct drive, the beam spots should be as large as possible, to maximize beam overlap to ensure drive uniformity, leading to lower single-beam intensities.

The gains for LPI's that are driven by single-beam interaction can be computed by ray-based methods.<sup>35,36</sup> For indirect drive, the largest single-beam gains correspond to stimulated Raman scattering (SRS) on the inner cone of beams deep inside the hohlraum and to stimulated Brillouin scattering (SBS) from the outer beam cones near the hohlraum wall.<sup>37</sup> For direct-drive designs, the single-beam gains/thresholds are not generally exceeded—a result of the lower beam intensities and the shorter plasma scale lengths relative to indirect drive.

In both approaches, there are ample opportunities for multibeam instabilities. In indirect drive, all beams from one side must overlap to get through the LEH, and the two rings of the inner cone overlap well into the hohlraum's interior. In direct drive, beams overlap everywhere in the underdense corona with a wide range of crossing angles. An understanding of the degree to which different beams can become cooperatively unstable with respect to LPI's is now realized to be crucial.

### Three-Wave Interactions

Unmagnetized plasmas support EM waves, electron plasma waves (EPW's), and ion-acoustic waves (IAW's).<sup>3</sup> The incident laser light is the source of large-amplitude EM waves. The quadratic nonlinearities associated with the plasma response, in the coronal or hohlraum plasma, result in the coupling between a given EM wave and the other linear waves supported by the plasma. As will become evident later, interactions that involve the coupling of three waves are seen as the most important for current ignition experiments.

A parametric instability involving three waves is possible when the frequency- and wave-number-matching conditions are satisfied:

$$\omega_0 = \omega_1 + \omega_2, \quad (1)$$

$$\vec{k}_0 = \vec{k}_1 + \vec{k}_2, \quad (2)$$

where  $\omega_i$  and  $\vec{k}_i$  ( $i = 0,1,2$ ) are the frequencies and wave numbers satisfying the dispersion relation for the  $i$ th wave. Typically, wave “0” represents the large-amplitude (pump) wave that drives the instability, while waves “1” and “2” are the decay (or daughter) waves.

The particular form of instability for coherent waves satisfying the matching conditions [Eqs. (1) and (2)] can be determined by solving the canonical coupled-mode equations.<sup>38,39</sup> Schematically, these are

$$L_0 A_0 = i\gamma_0 A_1 A_2, \quad (3)$$

$$L_1 A_1 = i\gamma_1 A_0 A_2^*, \quad (4)$$

$$L_2 A_2 = i\gamma_2 A_0 A_1^*, \quad (5)$$

where  $L_i$  represents the linear propagator for wave  $i$ ,  $A_i$  is the corresponding wave action (related to the wave amplitude), and the  $\gamma$ 's are the coupling constants that depend on the wave type.<sup>39</sup> Instability, if present (i.e., wave growth is sufficient to overcome the effective dissipation or damping), can be either absolute or convective. Absolute instability corresponds to unstable eigenmodes that grow temporally, while convective instability is limited to spatial amplification.<sup>40–42</sup> The effects of plasma inhomogeneity, or deviation from exact resonance, result in the appearance of phase factors on the right-hand side of Eqs. (3)–(5). Plasma inhomogeneity, which is always present experimentally (see Fig. 137.50), introduces a threshold condition on the intensity of the pump wave. Absolutely unstable couplings can become convective in its presence. The expression for Rosenbluth gain<sup>43</sup> is the most well-known:

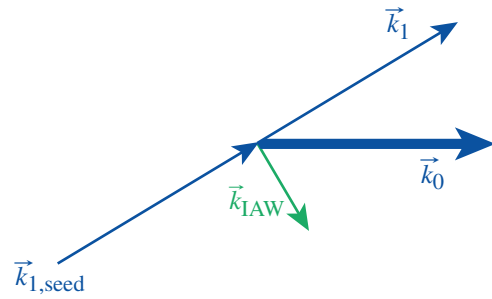
$$A_1 = A_{1,\text{seed}} \exp(G), \text{ where } G = \frac{2\pi\gamma^2}{|\kappa' V_{g,1} V_{g,2}|}, \quad (6)$$

which describes the finite amplification of wave amplitudes arising from wave convection out of the region where the three waves are resonantly matched [i.e., where Eqs. (1) and (2) are satisfied]. The gain exponent  $G$  depends on the square of the homogeneous temporal growth rate  $\gamma$ , the spatial derivative of the phase mismatch  $\kappa' = \partial/\partial x (\vec{k}_0 - \vec{k}_1 - \vec{k}_2)$ , where  $x$  is the direction of the inhomogeneity, and the group velocities of the two daughter waves,  $V_{g,i}$ . If the gain is large enough, the seed large enough, or the instability absolute, it will no longer be possible to neglect nonlinear effects such as particle trapping, nonlinear frequency shifts, harmonic generation, etc., which are not described by Eqs. (4) and (5). In this case, one must

often resort to numerical calculations of the type discussed in **Numerical Investigations of Multibeam TPD** (p. 72).

The following possibilities are specific to the case where the primary wave (0) is a large-amplitude EM wave: SBS results when the decay waves are EM and ion acoustic; SRS when they are EM and electron plasma waves; and two-plasmon decay (TPD) when both decay waves are EPW's. The decay into an EPW and an IAW can occur, but it is not seen to be important, while decay into two EM waves or two IAW's is not possible.

There are several ways in which multiple beams can cooperate to produce instability of the above types. Daughter waves can be shared between decays occurring in different beams<sup>44</sup> or instability can be seeded (or induced) because one of the daughter waves is present, either in the laser drive or as a result of decays occurring elsewhere in the plasma (see Fig. 137.51).<sup>45</sup> In this way, rescatter and multibeam amplification of backscatter can occur.<sup>46</sup> When daughter waves can be shared, the growth rates (or convective gains) can be expected to depend on the combined EM wave intensities.<sup>44</sup>



TC11003JR

Figure 137.51

Wave-vector diagram for cross-beam energy transfer. The decay of the pump electromagnetic (EM) wave (with wave vector  $\vec{k}_0$ ) into an ion-acoustic wave ( $\vec{k}_{\text{IAW}}$ ) and a scattered-light wave ( $\vec{k}_1$ ) is induced because the light wave  $\vec{k}_{1,\text{seed}}$  is already present at levels greatly exceeding the thermal noise.

Although filamentation has been a concern, particularly for indirect drive, and important work has been done to understand filamentation driven by multiple beams<sup>47,48</sup> and the related effect of beam bending,<sup>49,50</sup> which was experimentally confirmed,<sup>51</sup> it will not be described here.

Cross-beam (or multibeam) interactions in plasmas and their potential uses have quite a long history. Examples include the beat-wave generation of EPW's<sup>52</sup> or IAW's<sup>53</sup> by crossing EM beams, or four-wave mixing and phase conjugation.<sup>53,54</sup> More

recently there has been great interest in the use of cross-beam interactions to achieve laser-pulse compression<sup>55</sup> or Raman amplification.<sup>46,56,57</sup> These topics are beyond the scope of this article and will not be discussed nor will many other subscale experiments or theory that were performed under conditions that are not directly relevant to ICF ignition. The recent review articles by Kirkwood<sup>46,58</sup> address these.

## Cross-Beam Energy Transfer

### 1. Description of the Mechanism

Cross-beam energy transfer (CBET) can be thought of as an induced SBS process,<sup>45</sup> occurring when multiple EM waves of similar (or equal) frequencies overlap in a plasma. This can be understood most simply for the case of two crossing plane EM waves (“beams”) of frequencies  $\omega_0$ ,  $\omega_1$  and wave vectors  $\vec{k}_0$ ,  $\vec{k}_1$ , respectively (Fig. 137.51). Therefore, with reference to Eq. (2), both wave vectors  $\vec{k}_0$  and  $\vec{k}_1$  are EM waves (defined by the illumination geometry), while  $\vec{k}_2 \equiv \vec{k}_{IAW}$  is the wave vector of an IAW defined by  $\vec{k}_{IAW} = \vec{k}_0 - \vec{k}_1$ .

The frequencies (or, equivalently, wavelengths) of the overlapping EM beams (i.e.,  $\omega_0$  and  $\omega_1$ ) control the proximity of the plasma response at the frequency  $\omega_0 - \omega_1$  to the ion-acoustic resonance  $\omega_2$ ,

$$\omega_0 - \omega_1 = \omega_2 \equiv \omega_{IAW} = \pm c_s \left| \vec{k}_{IAW} \right| + \vec{v} \cdot \vec{k}_{IAW}. \quad (7)$$

Here  $c_s$  is the ion-acoustic speed and  $\vec{v}$  is the plasma (hydrodynamic) flow velocity. At (or near) resonance, the system [Eqs. (3)–(5)] becomes parametrically unstable (convectively), and substantial power can be transferred from the higher-frequency EM wave to the lower-frequency wave (where “higher” and “lower” refers to the frequencies determined in the reference frame where the plasma flow velocity vanishes). Energy transfer can occur if both laser beams have the same frequency (wavelength) in the presence of a Mach-1 flow ( $|\vec{v}| \sim c_s$ ) aligned with  $\vec{k}_{IAW}$ .

Interest arising from indirect-drive ICF (see the next subsection) stimulated a great deal of both theoretical/numerical<sup>34,45,59–63</sup> and experimental<sup>64–72</sup> activity in CBET starting in the mid-90s. Experiments were performed for frequency-mismatched beams<sup>67,73</sup> and equal-frequency beams.<sup>65,68,69,72,74,75</sup>

### 2. SBS-Mediated CBET in ICF Experiments

The potential importance of induced SBS (CBET) was recognized early in both indirect- and direct-drive approaches to ICF. Haan’s paper in 1995 (Ref. 31) cites forward SBS resulting in energy transfer between the NIF beam cones (Fig. 137.48) as a concern for indirect drive. At the time, the baseline pro-

posal for indirect drive on the NIF incorporated a four-color scheme that was proposed as an option for the control of LPI’s occurring in the hohlraum.<sup>31</sup> Kruer showed theoretically that the intensity and frequency separation of the beams in this baseline proposal were such that ion waves could be driven resonantly, causing a significant energy transfer among the beams.<sup>45</sup> Kruer’s calculations highlighted the effectiveness of detuning by wavelength shifting the NIF beams and determined that nonlinear effects would not play a strong role in limiting energy transfer for the parameters of interest. The ability to induce a wavelength shift between the two beam cones was implemented on the NIF, specifically to reduce vulnerability of the NIF point design to this energy transfer.<sup>34,76,77</sup> In practice, the frequency shift was applied to the outer cones, resulting in a “two-color” capability that could be used to prevent unwanted changes to the illumination symmetry caused by CBET. The frequency shifts were chosen to be sufficient to prevent IAW resonances inside the beam-crossing volume (see **Indirect Drive**, p. 59 and Fig. 137.50).

In the context of direct drive, Randall *et al.*<sup>78</sup> showed that unabsorbed light reflected from the critical surface could act as an EM seed to induce SBS in the corona. The importance of cross-beam interactions in direct-drive implosions on OMEGA was first investigated experimentally by Seka,<sup>79</sup> and numerical investigations of these experiments were performed in two dimensions using the paraxial *pF3D* code<sup>80</sup> and a non-paraxial model.<sup>81</sup> It was not possible to make more-general 3-D numerical calculations of the kind made for indirect drive (and described later in **CBET in Indirect Drive on the NIF**, p. 64)<sup>76,77</sup> because the complex beam geometries precluded the use of the paraxial approximation for the crossing beams.

A detailed spectroscopic analysis of the scattered light in spherical implosion experiments was performed on OMEGA, and the spectral shifts were compared with the expected Dewandre shift,<sup>82</sup> arising from the time-varying optical path, based on *LILAC*<sup>83</sup> predictions for the hydrodynamic profiles assuming collisional absorption<sup>3</sup> of the laser light alone.<sup>84</sup> This provided experimental evidence of the CBET effect in spherical implosion experiments.<sup>84–87</sup> The spectroscopy helped guide the development of a ray-based model of CBET that generalized Randall’s earlier analysis to the complex illumination geometry present in direct-drive experiments (Fig. 137.50).<sup>84–87</sup> The model solves the coupled-mode equations [Eqs. (3)–(5)] pairwise along rays, making use of the strong damping approximation for the IAW, which is physically motivated and makes the model practical to implement. Reference 35 gives a detailed description of ray-based calculations in indirect drive.

CBET has turned out to be of major significance in ICF experiments over the past few years, both in direct- and indirect-drive geometries. Because of differences in the drive (**Comparison of LPI Between Indirect-Drive and Polar-Drive Schemes**, p. 60), its behavior is somewhat different in each case and is described separately below.

**a. CBET in direct drive.** When a detailed ray-based CBET model was self-consistently incorporated into one-dimensional (1-D) radiation-hydrodynamics calculations (*LILAC*<sup>83</sup>), its impact on target performance for spherically symmetric implosions could be computed and compared with OMEGA experimental data.<sup>88,89</sup>

It was realized that, in direct drive, CBET preferentially transfers energy from the central portion of each laser beam to the outer portions (or “wings”).<sup>85,90</sup> Light rays in the wings of each beam, with large impact parameters, are not well absorbed and turn at densities below critical<sup>3</sup> (e.g., the purple ray in Fig. 137.52). On their outward trajectory, after turning, these rays cross incoming rays (e.g., the blue ray in Fig. 137.52), where they provide an enhanced EM seed for SBS side- or backscatter (Fig. 137.51). Since the hydrodynamic flow velocity is directed radially outward in the underdense corona, the outgoing rays are red shifted relative to the incoming rays in the frame where the plasma is locally at rest. If all beams have the same frequency in the lab frame, the energy transfer is directed from the incoming rays to the outgoing rays (shown schematically by the green arrow in Fig. 137.52). This represents a loss in laser coupling. The process becomes resonant near the Mach-1 surface, for equal-frequency beams (in the lab frame) [Eq. (7)], although the gains are small because of the strong radial gradients in flow velocity [large  $\kappa'$  in Eq. (6)]. The EM seed provided by the reflected light is very large relative to thermal fluctuation levels, so even small gains can have a significant effect on the absorbed energy.

The best agreement between 1-D *LILAC* calculations and measured absorption and scattered-light spectra was obtained for OMEGA spherical implosions when the CBET model was used in conjunction with nonlocal thermal transport.<sup>88,89,91</sup> Figure 137.53 compares the (a) measured and the calculated implosion trajectory with (b) the scattered power for a spherical implosion on OMEGA (shot 63912).

The implosion trajectory (defined as the radius of the ablation surface as a function of time), which is a gauge of the hydrodynamic efficiency of the target, is inferred from x-ray self-emission images,<sup>92</sup> while the time-dependent laser

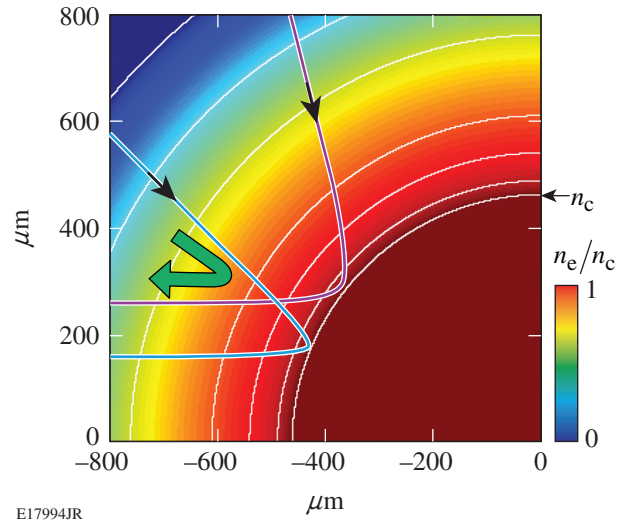


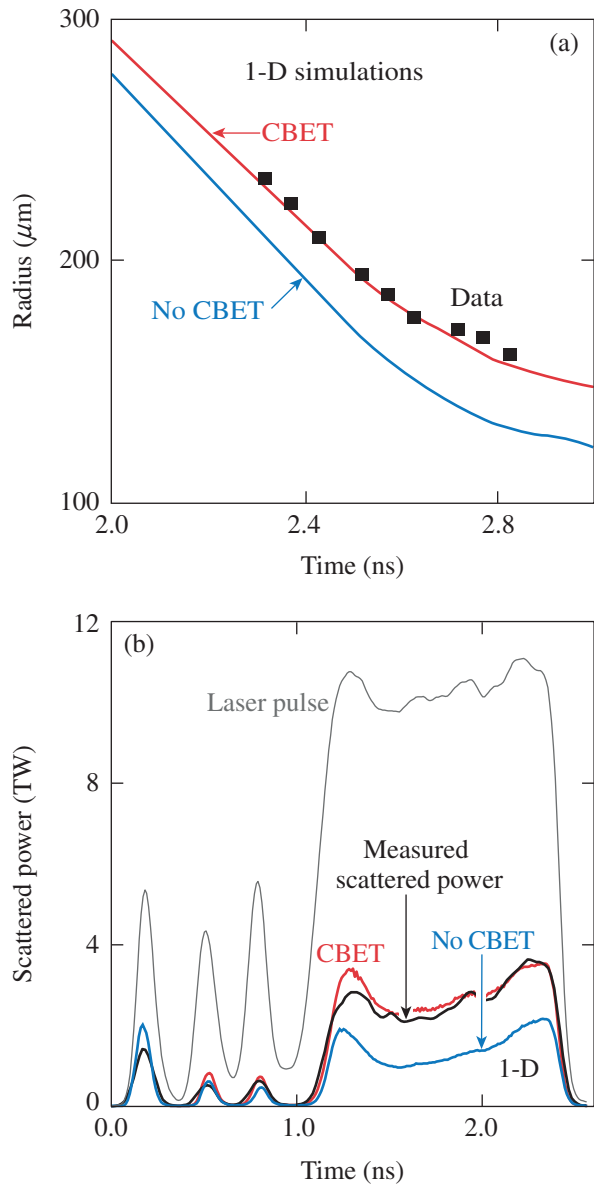
Figure 137.52

The coronal electron density  $n_e$ , normalized to the critical density  $n_c$ , is plotted in one quadrant of an OMEGA-scale spherically symmetric implosion. Two sample ray trajectories (shown as blue and purple lines) serve to illustrate the transfer of beam energy (see text).

absorption fraction and scattered-frequency spectra (not shown) tightly constrain the laser coupling.<sup>87</sup> Both of these observables are well matched by the 1-D *LILAC* CBET model, while calculations with collisional absorption alone fail to reproduce the results (Fig. 137.53).

These observations led to the conclusion that between 10% to 20% of the laser drive could be lost relative to expectations based on collisional absorption alone. This motivated further work to test the predictions of these models and to search for mitigation strategies.<sup>89,93</sup> Experiments were performed on OMEGA that demonstrated the expected enhancement in laser coupling in implosions with narrow-beam illumination relative to the target size.<sup>89,93</sup> The effect of narrowing the beam is to reduce the EM seed (the purple rays in Fig. 137.52) and mitigate the CBET effect. Mitigation strategies are discussed in more detail in **Mitigation of Multibeam Instabilities** (p. 74).

**b. CBET in indirect drive on the NIF.** The first comprehensive assessment of CBET in indirect drive was made prior to the NIF ignition campaign using a 3-D steady-state paraxial model for the nonlinear interaction between pairs of NIF quads.<sup>76,77</sup> The energy transfer between the NIF beam cones was calculated by summing the contribution from nearest-neighbor quads in the forward-scattering geometry (a geometry similar to that shown in Fig. 137.51) (this was predicated on the interquad power transfer being small). The nearest-neighbor interaction was greatly simplified because



E21315JR

Figure 137.53

(a) The implosion trajectory for a spherical implosion on OMEGA (shot 63912). The experimentally determined trajectory (solid squares) is compared against two 1-D *LILAC* calculations: collisional absorption of laser light only (blue curve) and the CBET model (red curve). (b) The scattered power as a function of time. The solid black curve is the measured scattered power and the red (blue) curves are the corresponding *LILAC* predictions. The laser pulse shape is shown for reference.

neighboring quads are close in angle ( $<14^\circ$ ) (Fig. 137.48), which permitted a paraxial treatment of the beam propagation (such an approximation is invalid for the direct-drive geometry). (The induced SBS process is forward scattering for indirect drive, unlike the dominant process in spherically symmetric drive where it is predominantly backscatter.) These calculations took

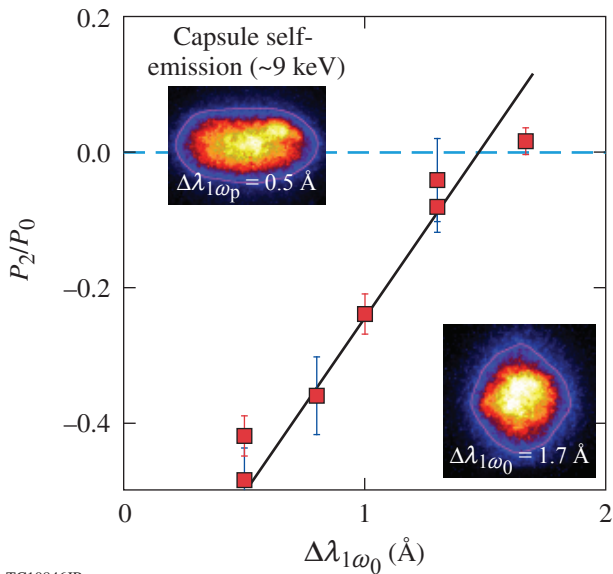
into account the expected hohlraum hydrodynamics conditions (obtained with *LASNEX*<sup>8</sup>) and laser-beam smoothing.<sup>76,77</sup>

The energy transfer in these calculations reached significant levels ( $\geq 15\%$ ) because of the high laser intensities and the long propagation distances over which the coupling takes place (**Comparison of LPI Between Indirect-Drive and Polar-Drive Schemes**, p. 60), despite the forward SBS coupling being off resonance [Eq. (7) is not satisfied]. (Note: In direct drive, the interaction distance is much shorter but the coupling is resonant.) The ion-wave amplitudes remained small  $\delta n/n \approx 10^{-4}$ , which justified the neglect of nonlinearity in the IAW response.<sup>34</sup>

These calculations indicated that the two-color scheme [wavelength shifting of the outer cone relative to the inner cone (**SBS-Mediated Cross-Beam Energy Transfer in ICF Experiments**, p. 63)] could mitigate CBET to a level sufficient to maintain the required implosion symmetry while keeping the coupling in the linear, or small-gain, regime. At the same time, it was foreseen that CBET could be used for symmetry control (by shifting laser power between the beam cones) if the margin for cone balance<sup>94</sup> on the laser system was limited for some reason.<sup>76,77</sup>

With the first experiments of the ignition campaign in 2009 (~200-TW “emulator” targets),<sup>95</sup> it became clear that the NIF cone fraction was unsuitable for creating symmetric implosions. The cone fraction, defined as the ratio of inner-cone energy to the total energy, needed to be 40% to 45% to obtain a round implosion.<sup>32</sup> This could not be achieved because the inner beams did not propagate to the hohlraum wall as well as expected,<sup>4,96</sup> and the cone fractions could not be adjusted to compensate for the loss related to power limitations of the inner cone of beams.

It was experimentally demonstrated that wavelength shifting could be used to compensate for the impaired propagation of the inner beams.<sup>4</sup> Figure 137.54 shows two snapshots of the capsule x-ray self-emission at the time of peak emission. The pole–equator asymmetry variation is measured by the ratio of the second- to the first-Legendre polynomial coefficients  $P_2/P_0$  in the spherical harmonic expansion of the x-ray flux isocontours from the self-emission images. Note that the hohlraum axis is vertical in these images, as in Fig. 137.48. Figure 137.54 shows that the implosions were oblate ( $P_2 < 0$ ) for small wavelength shifts,  $P_2/P_0$  varied linearly with the wavelength shift, and implosions became round ( $P_2 = 0$ ) at  $\Delta\lambda \approx 1.7 \text{ \AA}$  (at  $1\omega_0$ ).



TC10846JR

Figure 137.54

Experimental demonstration of symmetry tuning by cross-beam energy transfer (figure taken from Ref. 4). The second Legendre ( $P_2$ ) coefficient of the x-ray self-emission contour (purple line on inset figures) increases linearly with wavelength separation between the inner and outer beam cones  $\Delta\lambda$ , becoming zero (“round”) at  $\Delta\lambda = 1.7 \text{ \AA}$  (at  $1\omega_0$ ).

The linear dependence of the  $P_2/P_0$  symmetry with wavelength was predicted by a simpler CBET model that was developed for use in “rapid assessment.”<sup>96</sup> While this model neglected refraction and the beam speckle structure/smoothing of the earlier paraxial work, the coupling of all quads was calculated simultaneously, i.e., all interquad couplings were computed, including pump depletion. As before, *LASNEX*<sup>8</sup> (or *HYDRA*<sup>97</sup>) hydrodynamics were used, but the hydrodynamics were not evolved self-consistently (cf., e.g., direct-drive calculations described in **CBET in Direct Drive**, p. 64). These calculations using the linear response of an ion wave to the beat ponderomotive force were in reasonable agreement with the 2009 experiments where NIF was operating at 200 TW of peak laser power with small wavelength shifts ( $\Delta\lambda = 1.5$  to  $5 \text{ \AA}$  at  $1\omega_0$ ), leading to small amounts of transfer. When the NIF reached its design energy (laser powers in the range of 400 to 500 TW), combined with changes to the LEH (CH liners were removed modifying the flow structure), the  $\Delta\lambda$  required to achieve good symmetry became very large ( $\Delta\lambda = 6$  to  $9 \text{ \AA}$  at  $1\omega_0$ ) as did the energy transfer.

The successful demonstration of outer- to inner-beam energy transfer for  $P_2$  symmetry control was followed by a demonstration of two successive CBET steps.<sup>11,32</sup> This involved an additional transfer step between the two rings of quads that

comprise the inner cone (Fig. 137.48), which was accomplished by introducing a second wavelength shift (i.e., three colors).

For the three-color operations on the NIF, the wavelength of the  $23.5^\circ$  quads was placed between that of the outer cone and the  $30^\circ$  inner cone of beams. As before, power was transferred from the outer quads to the inner quads near the LEH (where all quads overlap) to maintain  $P_2$  symmetry. Because of the second frequency shift, the  $23.5^\circ$  quads were higher in frequency compared to the  $30^\circ$  quads and a second transfer (from the  $23.5^\circ$  to the  $30.0^\circ$  quads) occurred deeper in the hohlraum when the outer cones had separated (the separation can be seen in Fig. 137.48).

This redirection of energy toward the  $23.5^\circ$  quad was motivated by experimental evidence that showed a decrease in laser–target coupling as energy was transferred to the inner beams as a result of SRS. This was not unexpected since the inner cones are the most prone to SRS backscatter instabilities (see **Stimulated Raman Scattering in Indirect Drive**, p. 67). However, the loss was specifically identified as resulting from increases in SRS on the  $23.5^\circ$  quads.<sup>32</sup> Redirecting energy from the  $23.5^\circ$  quads to the  $30^\circ$  quads (keeping the inner-cone energy constant) before the SRS gain region (p. 67) decreased backscatter and improved the coupling to the target, thereby increasing the radiation drive.<sup>11,32</sup>

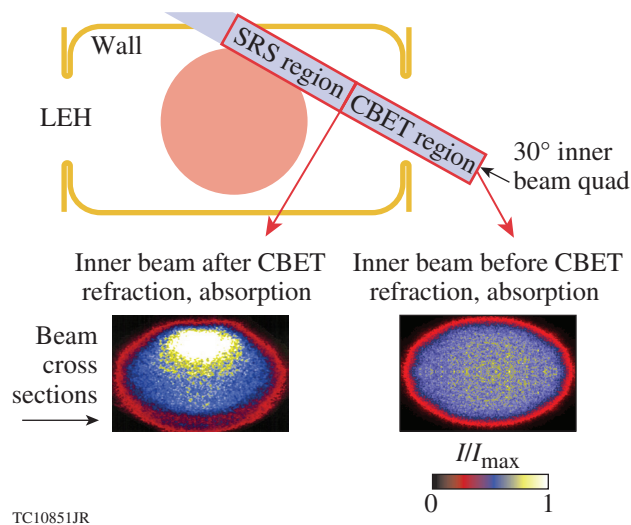
Although the ignition campaign started out in the linear gain regime and the models had a good degree of predictability, it ended with large gains and the linear models were no longer predictive.<sup>32,98,99</sup> Indeed, the linear calculations fail to reproduce the experimental observables, and usually predict full pump depletion of the outer beams, which has never been observed.<sup>98,99</sup> To obtain an integrated working model, an *ad hoc* adjustment parameter was applied to the density response: a saturation amplitude of  $\delta n/n = 3$  to  $4 \times 10^{-4}$  (Ref. 32). Michel *et al.*<sup>98,99</sup> have recently shown that stochastic ion heating can occur when multiple laser beams overlap in plasma. The electrostatic field created in response to the ponderomotive force of multiple overlapping beams was shown to transfer energy and momentum to the ions. For typical NIF conditions, it was calculated that such stochastic heating is an important mechanism driving hydrodynamic evolution in the beam-overlap region. The modifications to the ion temperature were predicted to reduce the CBET linear gains by a factor of 4 to 5 over the course of a nanosecond. Such considerations may remove the *ad hoc* density saturation parameter and restore agreement with experimental observations. In this same work, a simplified model of the effect in a form suitable for inline

implementation in hydrocodes was presented (see comments in the **Introduction**, p. 58).

### Interactions in Competition with CBET

In laser-driven fusion experiments, CBET occurs before the laser beams have fully deposited their energy in the target (i.e., the walls of the hohlraum in indirect drive or at the critical surface in direct drive).

In indirect drive, CBET occurs in the beam-overlap region near the LEH (as previously described). Gain calculations show that backscattering and filamentation instabilities occur deeper in the hohlraum, outside of the volumes where the beams cross and transfer energy.<sup>76</sup> SRS in the NIF hohlraum has been identified to occur midway between the LEH and the hohlraum wall along the path of the inner beam cones (Fig. 137.55).<sup>37</sup> All potential interactions taking place in the hohlraum's interior are therefore “downstream” of CBET. An understanding of these downstream instabilities should take into account not only the changes in hydrodynamics caused by CBET but also the angular and spatial redistribution of energy within the beams. These problems highlight the complexity of LPI's in general and show how the nonlocal and scale mixing can occur between the macroscopic (hydrodynamic) and microscopic (plasma physics) scales.



TC10851JR

Figure 137.55

A drawing showing the path of a 30° inner-cone quad as it propagates from the LEH to the wall of a NIF hohlraum. The spatial regions where CBET and SRS occur are indicated. The intensity of the quad is shown, in cross section, just before entering the LEH and after propagation through the CBET region. The increase in the quad intensity is not spatially uniform.<sup>100,101</sup> (Figure taken from Ref. 101.)

Figure 137.55 shows an example of how these problems can be tackled through the sequential combination of multiple numerical models. The intensity of a 30° inner-cone quad is shown, in cross section, both before and after the energy transfer has occurred. CBET distorts the transverse intensity profile of the laser beam and gives rise to an effective shift in pointing.<sup>77</sup> The propagation from the LEH to the region where SRS occurs, including refraction, absorption, and CBET, has been calculated using a steady-state paraxial model.<sup>96</sup> When the SRS gain region is reached, the spatially dependent laser intensity is used as input for a second calculation using the code *pF3D*, which is able to compute the SRS coupling (the results of these types of *pF3D* calculation are discussed in the next subsection). Both of these stages assume plasma hydrodynamic profiles calculated using *LASNEX* (or *HYDRA*). The self-consistency between LPI calculations and hydrodynamics calculations was discussed previously in **CBET in Direct Drive** and **CBET in Indirect Drive on the NIF** (p. 64).

Similar arguments are expected to apply in directly driven targets, although the degree of spatial separation between different instability regions is less clear. The correct modeling of CBET is a prerequisite for the understanding of instabilities occurring deeper in the target. The most important of these are considered to be SRS (in indirect drive) and two-plasmon decay (in direct drive).

### 1. Stimulated Raman Scattering in Indirect Drive

Analyses of SRS prior to the NIF ignition campaign were based mostly on the computation of single-beam gains and beam propagation<sup>31,35,102</sup> that were tested in subscale OMEGA experiments.<sup>103,104</sup> The results suggested that tolerable levels of SRS were to be expected. However, SRS from the inner cones of NIF hohlraums was routinely observed during the ignition campaign, with reflectivities of the order of 20% ( $E_{\text{SRS}} \geq 100$  kJ) (Ref. 95). As a result, SRS is the primary LPI mechanism responsible for the reduction in energy coupling in the hohlraum.<sup>95</sup>

A spectral analysis of SRS scattered light [diagnosed in a full-aperture backscatter station (FABS) on the 30° inner cone]<sup>105</sup> pointed to lower hohlraum temperatures than predicted, which in part motivated an assessment of the way plasma conditions were calculated. This reassessment led to the implementation of the detailed configuration accounting (DCA)/high-flux (HF) model in hydrodynamic modeling.<sup>106,107</sup> With the HF model, SRS was predicted to occur halfway between the LEH and the hohlraum wall (Fig. 137.55), where there is still overlap between the inner cones, instead of closer to the wall,

where there is none (as earlier predictions had suggested).<sup>102</sup> This new model removed the gross discrepancies between SRS observations and predictions.<sup>37</sup>

The modification in plasma conditions, as predicted by the HF model, did not fully explain the SRS spectra from the inner quads. It was noticed that a discrepancy between linear single-beam gains and the observed spectra of SRS light could be improved by combining the intensities of neighboring beams/quads. When the overlap intensity of the 23.5° and 30° quads was included in SRS gain calculations (**Three-Wave Interactions**, p. 61), agreement with the experimental SRS scattered-light spectrum was improved.<sup>37</sup> It seems likely that multibeam SRS occurs through the sharing of the EM decay waves where the two inner cones overlap [Fig. 137.56(a)].<sup>37</sup>

A “proof-of-principle” calculation to test this multibeam effect was performed by simulating the propagation of two<sup>37</sup> and three<sup>101</sup> overlapping quads using the code *pF3D* (as described above in **Interactions in Competition with CBET**, p. 67). The three overlapped quads used to initialize *pF3D*

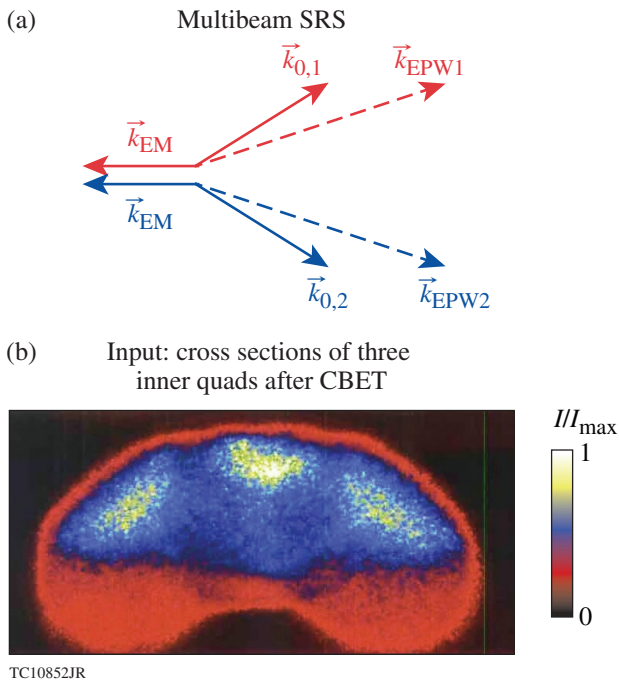


Figure 137.56

(a) A wave-vector decay diagram for SRS occurring in two beams (with wave vectors  $\vec{k}_{0,1}$  and  $\vec{k}_{0,2}$ ) that share a common backscattered electromagnetic wave ( $\vec{k}_{EM}$ ). The two electron plasma waves ( $\vec{k}_{EPW1}$  and  $\vec{k}_{EPW2}$ ) are not shared. (b) Cross sections of the spatial intensity profile of three overlapping NIF inner-cone quads. The sharing of scattered EM waves is possible where there is significant overlap between beams (lower panel was taken from Ref. 101).

calculations of multibeam SRS are shown in Fig. 137.56(b). A 30° quad at the center overlaps with two 23.5° quads (one on either side). The *pF3D* calculations demonstrated that the quads can share a reflected SRS light wave to which they resonantly match through separate electron plasma waves [Fig. 137.56(b)]. Furthermore, multibeam (three-quad) predictions for the SRS reflectivity on the diagnosed 30° quad approached measured values.<sup>101</sup>

While these results are compelling, *pF3D* is a fluid-based code and it is possible that some discrepancies may be kinetic in origin. It would be interesting to see how multibeam kinetic calculations (e.g., including effects of the type described recently by Chapman *et al.*<sup>108</sup> and Yin *et al.*<sup>109–111</sup>) affect agreement between multibeam predictions and measurements.

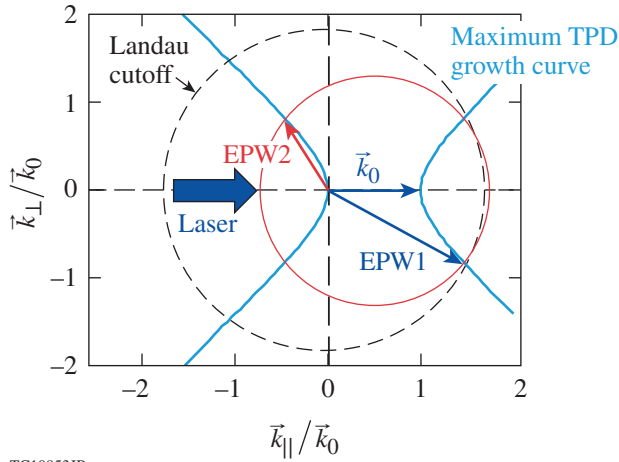
## 2. Two-Plasmon Decay (TPD) in Directly Driven ICF

TPD has been observed in the blow-down of the LEH windows in indirect drive,<sup>112</sup> but it is generally considered to be more important for direct drive,<sup>113</sup> where it is undesirable because of the anomalous absorption of laser light at densities below the critical density and the potential to accelerate electrons to high energies.<sup>114–118</sup> High-energy electrons can preheat the target and severely degrade performance since efficient implosions require the fuel to remain on a low adiabat.

TPD<sup>43,119–123</sup> is a three-wave-decay instability in which an EM wave parametrically decays into two longitudinal EPW’s in the neighborhood of the quarter-critical density surface (**Three-Wave Interactions**, p. 61). Its decay diagram is shown schematically in Fig. 137.57 for a single-plane EM wave pump. As described in on p. 61, the three waves satisfy the frequency- and wave-number-matching conditions [Eqs. (1) and (2)]. These conditions, together with the dispersion relations for the EM wave [ $\omega_0^2 = \omega_{pe}^2 + c^2 |\vec{k}_0|^2$ ] and the EPW’s

$$\omega_{EPW1}, \omega_{EPW2} = \pm \omega_{pe}^2 + 3v_{Te}^2 |\vec{k}_{EPW1, EPW2}|^2,$$

where  $\omega_{pe} = (4\pi n_e e^2 / m_e)^{1/2}$  is the electron plasma frequency, define the allowable wave vectors for decays at a given density. The decay wave vectors must lie on a sphere centered on  $\vec{k}_0/2$ , having a radius that is a monotonically decreasing function of the density (shown by the red circle in Fig. 137.57).<sup>124</sup> This defines the maximum density at which TPD can occur to be slightly below the quarter-critical density. Larger wave-number decays occur at lower densities, but for  $|\vec{k}| \lambda_{De} \gtrsim 0.25$ , i.e., beyond the Landau cutoff (dashed circle in Fig. 137.57), EPW’s are very heavily Landau damped [ $\lambda_{De} \equiv (T_e / 4\pi n_e e^2)^{1/2}$  is the electron Debye length].



TC10853JR

Figure 137.57

A wave-vector decay diagram showing the decay of a single EM plane-wave pump beam of wave vector  $\vec{k}_0$  into two EPW's having wave vectors  $\vec{k}_{\text{EPW1}}$  and  $\vec{k}_{\text{EPW2}}$  in the plane of polarization. The maximum growth rate for the instability in homogeneous plasma falls on a hyperbola which is parameterized by the electron plasma density. For a given density, decay wave vectors lie on a circle (red) and the most-unstable modes occur at the intersection of the red circle and the blue hyperbolas. The dashed line is the Landau cutoff  $|\vec{k}| = 0.25 k_D$ .

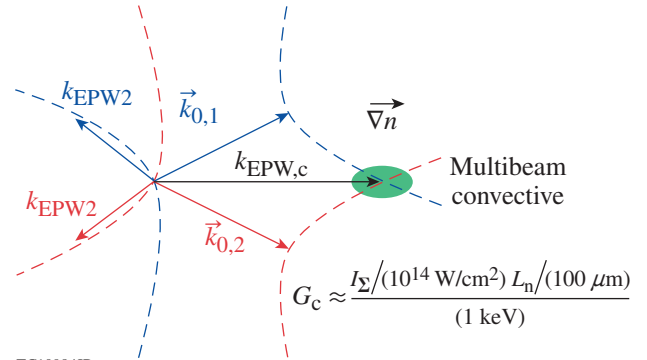
The linear stability of a single-plane EM wave subject to TPD in homogeneous plasma is well known.<sup>43,119–123,125,126</sup> The temporal growth rate  $\gamma_0$  for a decay of wave vector  $\vec{k}$  (in the absence of EPW damping) is given by

$$\gamma_0 = \frac{\vec{k} \cdot \vec{v}_{\text{osc}}}{4} \frac{[(\vec{k}_0 - \vec{k})^2 - k^2]}{k |\vec{k}_0 - \vec{k}|}, \quad (8)$$

where  $\vec{v}_{\text{osc}} = e\vec{E}_0/(\omega_0 m_e)$  is the oscillation velocity of an electron in the electric field of the plane EM wave  $\vec{E}_0$  (Ref. 3). The relation between  $k_{\parallel}$  and  $k_{\perp}$  (parallel and perpendicular components of  $\vec{k}$  with respect to  $\vec{k}_0$ ) corresponding to maximum growth defines a hyperbola in  $k$  space,  $k_{\perp}^2 = k_{\parallel}(k_{\parallel} - k_0)$  (shown by the solid blue hyperbolas in Fig. 137.57).

For homogeneous plasma, the square of the multibeam growth rate is the sum of the squares of the single-beam growth rates [Eq. (8)] for all beams ( $i$ ) that share a common (symmetric) decay EPW ( $\gamma^2 = \sum_i \gamma_{0,i}^2$ ) (Ref. 127). This is a general result for three-wave instabilities.<sup>44</sup> Figure 137.58 shows how two coherent, equal-frequency beams can share a common daughter EPW. It can be easily seen that the angle between the common wave  $\vec{k}$  vector ( $\vec{k}_{\text{EPW,c}}$ ) and the  $\vec{k}$  vectors of participating beams ( $\vec{k}_{0,1}$  and  $\vec{k}_{0,2}$ ) must be the same. Maximum growth

occurs when the single-beam maximum growth rate curves (the blue and red dashed hyperbolas in Fig. 137.58) intersect. This can occur only at a specific density.<sup>124</sup>



TC10984JR

Figure 137.58

A schematic TPD decay diagram for two overlapping EM waves (having  $\vec{k}$  vectors  $\vec{k}_{0,1}$  and  $\vec{k}_{0,2}$ ) whose bisector is in the direction of a constant gradient in plasma density  $\vec{\nabla}n$ . The multibeam homogeneous temporal growth rate is maximized for decays  $\vec{k}_{\text{EPW,c}}$  occurring at densities that correspond to the intersection of the individual maximum growth rate curves (red and blue dashed hyperbolas). Since these waves are often associated with large group velocity, a linear analysis predicts convective instability in the presence of the density gradient, and a common-wave gain can be computed.<sup>127</sup>

In plasma with a linear inhomogeneity in the electron plasma density, even the single-beam case is complicated. The linear variation in plasma density can be shown to lead to convective saturation for most decays,<sup>128</sup> leading to spatial amplification of unstable EPW's by the Rosenbluth gain [i.e., Eq. (6)]. A careful linear stability analysis of small wave-number decays, which are near their turning point (invalidating the Rosenbluth analysis), revealed the presence of absolute instability.<sup>120,123,125,129</sup> The threshold for the absolute instability was first calculated correctly by Simon *et al.*,<sup>123</sup> resulting (for conditions of relevance to direct-drive-ignition experiments) in an absolute threshold below the nominal convective threshold ( $G = 2\pi$ ) (Ref. 128). For a single beam, absolute instability involves small  $\vec{k}$ -vector decays and is restricted to a narrow region of densities in the neighborhood of the quarter-critical density. Larger wave-number decays are convectively unstable and occur at lower densities. The very restricted range of purely convective growth means that single-beam TPD is inherently nonlinear.<sup>130</sup>

The linear stability analysis of multibeam TPD in a linearly varying density profile is more complicated, but significant progress has been made recently. The case of convective multibeam decays has been described by computing the expression for the multibeam homogeneous growth rate and applying the

Rosenbluth gain formula [Eq. (6)].<sup>127,131</sup> This allows one to compute a “common-wave gain”  $G_c$  that depends on the density scale length, the electron temperature, and the combined intensity of beams that contribute to the symmetric common wave (Fig. 137.58). The common-wave gain has been used as a figure of merit in the analysis of multibeam experiments<sup>127</sup> and to compare experiments having different density scale lengths and temperatures.<sup>131</sup> This is reviewed in more detail in **Experimental Evidence of Multibeam TPD** below.

Detailed analyses have been performed for specific configurations of one to six EM beams by numerical integration of the fundamental TPD equations in both real space<sup>132</sup> and Fourier space.<sup>133</sup> An absolutely unstable cooperative multibeam instability was found to exist (for the same reasons as in the single-beam case). The origin of absolute instability for multibeam TPD is illustrated in Fig. 137.59. Figure 137.59 shows single-beam decays occurring in two beams. These decays involve a small  $\vec{k}$ -vector plasmon and can be absolutely unstable, with a threshold that has been computed by Simon *et al.*<sup>123</sup> These two decays share the small  $\vec{k}$ -vector plasmon and the decay can become cooperative. Results show that small wave-number decay EPW’s can often be shared among multiple beams. While the absolute multibeam threshold is found to depend on the specific beam configuration, it is generally below the common-wave convective threshold (as for a single beam).<sup>19,132</sup>

**Numerical Investigations of Multibeam TPD** (p. 72) on the nonlinear modeling of multibeam TPD saturation and hot-electron production gives more details regarding the implica-

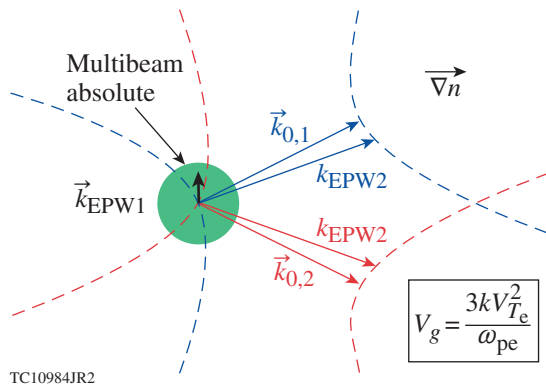


Figure 137.59

A wave-vector diagram for two crossing EM waves of wave vectors  $\vec{k}_{0,1}$  and  $\vec{k}_{0,2}$ . The single-beam maximum growth rate curves are shown schematically by the dashed hyperbolas, showing the region of cooperation (shaded in green). These decays can become absolutely unstable in inhomogeneous plasma because the small wave-vector EPW’s are near their turning point and have small group velocities (formula shown in inset).

tions of these results, particularly with regard to nonlinear stability and the applicability of Rosenbluth gain.

### 3. Experimental Evidence of Multibeam TPD

Experimentally, signatures of TPD have been observed in the ionosphere<sup>134</sup> and in LPI experiments.<sup>135,136</sup> For the most part, either these experiments were carried out with a single interaction beam or the analysis did not consider multibeam effects. Only recently have these experiments observed signatures of multibeam interactions. Some of these are described below.

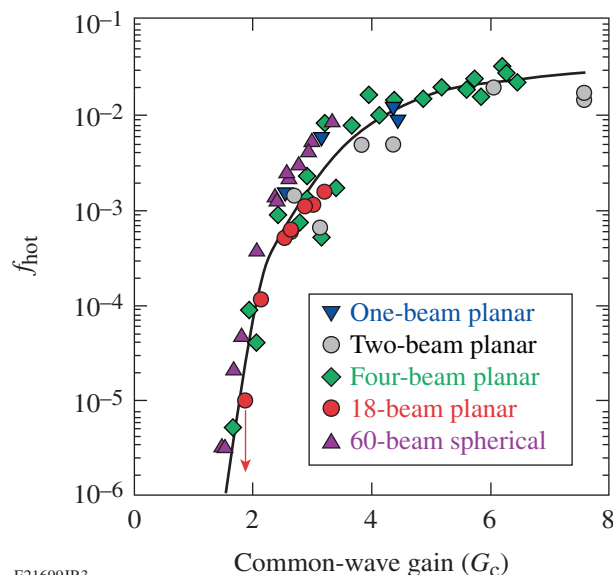
Several characteristic signatures of TPD instability include odd half-integer harmonics observed in the scattered light,<sup>136–144</sup> a hard component ( $>20$  keV) in the x-ray bremsstrahlung spectrum,<sup>116,145</sup> an energetic tail in the electron spectrum,<sup>114</sup> and  $K_\alpha$  emission from cold material.<sup>146,147</sup> Many of these experiments were carried out at the Omega Laser Facility.<sup>26</sup> In these experiments, the coincidence of the above TPD signatures, combined with the absence of SRS backscattered light, is considered evidence for the dominance of TPD instability.<sup>113</sup>

**a. Multibeam TPD experiments using hard x-ray measurements.** The multibeam nature of TPD in both planar and spherical targets was demonstrated on OMEGA in 2003 based on observations of hard x-ray bremsstrahlung.<sup>148</sup> X-ray bremsstrahlung is an indirect observation of TPD since it is produced by energetic electrons that have been accelerated in the electric field of TPD-produced EPW’s, most likely in the turbulent nonlinear state.<sup>149</sup> These 2003 experiments showed that the overlapped intensity (defined as the incoherent sum of the single-beam intensities) governed the hot-electron production, i.e., similar hard x-ray signals were obtained regardless of the number of beams involved, provided that the overlapped intensity was the same. It was proposed that overlapping beams could excite the same plasma wave. These results and more-detailed spectroscopic analysis were discussed by Seka *et al.* in 2009 (Ref. 113).

More recently, experiments on OMEGA EP were used to produce long plasma density scale lengths ( $\geq 300 \mu\text{m}$ ) and explore TPD driven by one to four beams.<sup>118,150</sup> These experiments quantified the hot electrons produced by measuring the  $K_\alpha$  emission excited in buried Mo layers, resulting in up to a few percent of the incident laser energy being converted to hot electrons at the highest laser intensities.<sup>150</sup> The idea of shared, or common, plasma waves was explored based on the concept of common-wave gain (Fig. 137.58).<sup>127,131</sup> A significant result was the demonstration that two beams, with similar polarization

directions, produce the same  $K_\alpha$  signal as one beam when the overlapped intensities are equal (similar to 2003). These experiments also demonstrated that four beams produce the same hot electrons as a single beam when the overlapped four-beam intensity is a factor of 2 higher—a result consistent with the expected reduction in growth rate based on common-wave considerations for the polarization of the OMEGA EP beams.<sup>127</sup> The hot-electron production from a variety of different targets (on both OMEGA and OMEGA EP) with varying scale lengths and temperatures was compared by plotting the inferred hot-electron fraction against the predicted common-wave gain for each configuration. Figure 137.60 shows the results taken from Ref. 131; when plotted against common-wave gain, a universal curve is obtained for the inferred hot-electron fraction.

**b. Optical signatures of multibeam TPD.** Optical signatures of TPD are important because, unlike scattering instabilities (such as SBS or SRS), the direct products of the decay (two EPW's) do not exit the plasma. Scattered light with frequencies near  $3\omega_0/2$  and  $\omega_0/2$  has been used to investigate TPD for many years.<sup>136–144</sup> Three-halves-harmonic emission ( $3\omega_0/2$ ) is generated by Thomson up-scattering of the incident laser light by TPD-produced plasma waves (i.e., self-Thomson scattering), or possibly by higher-order nonlinear processes. Half-harmonic emission ( $\omega_0/2$ ) can be generated in a variety of ways. These



E21699JR3

Figure 137.60  
Experimental observation of hot-electron production in both planar and spherical experiments on OMEGA/OMEGA EP (figure taken from Michel *et al.*<sup>131</sup>). The hot-electron production is inferred from a combination of hard x-ray bremsstrahlung and/or  $K_\alpha$  fluorescence.<sup>118</sup> This is plotted against the gain for common TPD EPW's (see Fig. 137.58).

include absolute Raman instability; the high-frequency hybrid instability, where the  $\omega_0/2$  light is a primary decay product; inverse resonance absorption; Thomson down-scattering; and inverse parametric decay of TPD plasmons, where the  $\omega_0/2$  light is generated as a secondary process.<sup>113</sup>

In Seka *et al.*<sup>113</sup> the onset of half-integer harmonic emission in spherical implosion experiments on OMEGA was observed to be consistent with the single-beam threshold of Simon *et al.*,<sup>123</sup> provided that the single-beam intensity in the threshold formula was replaced by the total overlapped intensity (i.e., by the incoherent sum of the intensities of all overlapping beams). Further analysis of the  $3\omega_0/2$  and  $\omega_0/2$  signatures led to the conclusion that the unstable EPW spectrum is much broader than would be expected on the basis of linear theory [see **Numerical Investigations of Multibeam TPD** (p. 72) for comparisons with nonlinear TPD theory]. While the EPW spectrum was determined to be broad, it was shown that the Landau cutoff is respected. Similar broad EPW spectra were inferred by Meyer and Zhu in early single-beam CO<sub>2</sub> laser experiments.<sup>139</sup>

As in earlier work,<sup>136</sup> the multibeam nature of TPD was not explored beyond the threshold observation. More recently, images of the half-harmonic emission from similar OMEGA experiments have been obtained.<sup>151</sup> Since the spatial regions that emit most brightly coincide with locations where multibeam TPD is expected to be driven most strongly, this has been interpreted as evidence of a multibeam effect in spherical implosion experiments.<sup>151</sup>

The most-direct observation of TPD EPW is obtained by Thomson scattering using a probe beam that is higher in frequency than the TPD interaction beam(s). For single-beam irradiation, the first such observations of TPD EPW's were obtained by Schuss *et al.*<sup>152</sup> and Baldis *et al.*<sup>153</sup> for CO<sub>2</sub> laser irradiation. The unstable TPD spectrum was determined by Meyer and Zhu using Thomson scattering, again for a single CO<sub>2</sub> interaction beam.<sup>139</sup> Very recently, Thomson-scattering experiments have been performed in multibeam planar experiments on OMEGA at 0.351  $\mu\text{m}$  using a  $4\omega$  (0.263- $\mu\text{m}$ ) Thomson-scattering probe beam.<sup>154</sup> Plasma waves were observed and found to be localized near the quarter-critical surface. The intensity of these EPW depended on the overlapped intensity of all the interaction beams.<sup>154</sup> These experiments promise to constrain numerical/theoretical predictions and provide a deeper understanding of multibeam interactions.

**c. Angular properties of hot-electron production by multibeam TPD.** The angular divergence of hot electrons produced

as a result of TPD instability is an important factor in determining hot-electron preheat in direct-drive experiments. In typical cryogenic direct-drive experiments,<sup>155</sup> the fast-electron energy deposited as preheat can be significantly less than the total energy of fast electrons produced. This is due to the factor-of-2 difference in radii between the cold shell and the quarter-critical surface.<sup>156</sup> It is therefore important to characterize the angular properties of hot electrons produced by multibeam TPD.

The directionality and energy spectrum of hot electrons produced by the TPD instability are difficult to predict because neither the saturated EPW wave-number spectrum nor the electron acceleration processes are well understood (see **Numerical Investigations of Multibeam TPD** below). The angular distribution of hot electrons and its dependence on the plane of polarization of a single-incident CO<sub>2</sub> laser beam were determined in early experiments by Ebrahim *et al.*<sup>114</sup> The results were obtained by measuring the spectra of hot electrons escaping the target at various angles. A strong peak in emission was observed at angles of  $\pm 45^\circ$  with respect to the wave vector of the incident light in the plane of polarization. This was thought to be consistent with the direction of the most-unstable TPD wave vectors for the parameters of the experiment [large wave-number decays consist of two plasmons propagating at angles of almost  $45^\circ$  and  $135^\circ$  with respect to the pump wave vector  $\vec{k}_0$  (see Fig. 137.57)]. Similar single-beam experiments with a  $0.351\text{-}\mu\text{m}$  interaction beam saw much weaker directionality, although emission was again stronger in the plane of polarization.<sup>116</sup>

Since the largest growth rates for multibeam interactions can involve TPD decay wave vectors that are symmetrically oriented with respect to the propagation direction of the interaction beams,<sup>127</sup> and experiments support the notion of common waves, a strong asymmetry might be expected in the direction of emission of hot electrons in multibeam experiments. An experimental technique was recently developed to estimate the angular divergence of hot electrons for conditions relevant to directly driven implosions.<sup>157</sup> Molybdenum-coated glass balls of varying diameters were suspended concentrically inside CH shell targets, which were then irradiated on the 60-beam OMEGA laser at intensities  $I \sim 1 \times 15 \text{ W/cm}^2$ . The hot-electron divergence was inferred from the dependence of the hot-electron-produced Mo  $K_\alpha$  signal on the varying diameter of the Mo shell (while maintaining similar interaction conditions in the underdense corona). The relative  $K_\alpha$  signal was best fit by a widely divergent hot-electron source, even after considerations of hot-electron recirculation,<sup>156</sup> scattering, and return-current instabilities were taken into account. The results of nonlinear

numerical models of TPD-produced hot electrons (described below) suggest possible reasons for these observations.

#### 4. Numerical Investigations of Multibeam TPD

Although advances have been made in understanding the linearized theory of multibeam TPD instability,<sup>21,127,128,131–133</sup> which are important for defining thresholds, linear theory alone is not sufficient. The presence of absolute instability guarantees that a nonlinear theory is necessary to describe its evolution beyond the picosecond time scale (i.e., nonlinear saturation) of importance to experiments that are several nanoseconds in duration. A nonlinear theory is required to describe hot-electron production and to interpret broad, odd half-harmonic emission spectra (see **Optical Signatures of Multibeam TPD**, p. 71).

Several numerical methods have been used to investigate the nonlinear evolution of TPD excited by a single EM wave. Since the TPD growth rate vanishes for decay wave vectors  $\vec{k}$  that are parallel to the pump wave vector  $\vec{k}_0$  [i.e.,  $\vec{k}_0 \cdot \vec{v}_{\text{osc}} = 0$  for EM waves in Eq. (8)], the instability must be studied in at least two dimensions. For a single EM wave, the maximum growth rate is obtained for decays in the plane of polarization (i.e., the plane defined by the vectors  $\vec{k}_0$  and  $\vec{v}_{\text{osc}}$ ); consequently, the majority of single-beam calculations performed to date have been two-dimensional (2-D) calculations in the plane of polarization. These include extended Zakharov models,<sup>130,137,156</sup> Zakharov models with quasilinear evolution of the electron distribution function,<sup>149</sup> explicit particle-in-cell calculations,<sup>129,158–161</sup> and reduced particle-in-cell (RPIC) techniques employing time enveloping.<sup>124,162,163</sup> These calculations have demonstrated the importance of ion-turbulence and profile modification in determining the saturated EPW spectrum<sup>158</sup> and hot-electron production.<sup>159</sup> For long-scale-length plasma relevant to ignition, the importance of collisional EPW damping has been noted, in both the linear and nonlinear turbulent states.<sup>149,159</sup> Although computationally challenging, several 3-D PIC calculations of single-beam TPD have been performed.<sup>164</sup>

Comparatively little work has been performed to investigate the nonlinear evolution of TPD excited by multiple beams. In two dimensions, RPIC calculations considered two crossed beams<sup>124</sup> and subsequent hot-electron production.<sup>162,163</sup> Calculations were performed with two EM waves arranged symmetrically about the density gradient with angles of  $\pm 23^\circ$ , both polarized in the simulation plane. These investigations determined the conditions for the existence of shared waves<sup>124</sup> and emphasized their importance in the nonlinear state. The scaling of hot-electron production with laser intensity was

obtained<sup>162</sup> and described in terms of “cavitating” Langmuir turbulence<sup>163</sup> (for a review of strong Langmuir turbulence see Robinson<sup>165</sup> or Goldman<sup>166</sup>). These RPIC calculations motivated the quasilinear Zakharov model of TPD, where in addition to solving the extended Zakharov equations of TPD, the spatially averaged electron-velocity distribution is evolved in the quasilinear approximation, self-consistently determining the Landau damping of the EPW’s.<sup>149,167,168</sup>

The extended Zakharov model of TPD is a fluid-based model that describes the nonlinear coupling between EPW’s and IAW’s. Figure 137.61 shows the results of a 2-D extended-Zakharov calculation of TPD driven by two overlapping EM waves, having a total intensity of  $1.2 \times 10^{14}$  W/cm<sup>2</sup>, taken from Zhang *et al.*<sup>19,169</sup> The density scale length is ignition relevant ( $L_n = 660 \mu\text{m}$ ), the electron temperature  $T_e = 2$  keV, and both EM waves are polarized in the plane (similar quasilinear calculations are described in more detail in Myatt *et al.*<sup>149</sup>). At early times  $t < 6$  ps the EPW spectrum is consistent with linear theory [Fig. 137.61(a)]. Both the convectively saturated common EPW and the absolutely unstable collective modes are observed. The common EPW’s can be seen close to  $\vec{k}/k_0 = (1.5, 0)$ , where the single-beam growth-rate curves intersect (cf. Fig. 137.58). The amplitude of these EPW’s has convectively saturated and is no longer growing. The bright “doublets” in the figure [ $\vec{k}/k_0 \sim (0, 0)$  and  $\vec{k}/k_0 \sim (0.9, \pm 0.4)$ ] correspond to the multi-beam absolute instability (cf. Fig. 137.59). These modes are

temporally growing and saturate only by nonlinear processes. For this particular case, the parameters set the absolute instability to be slightly above multibeam threshold, but the convective common wave is below threshold.

The late-time ( $t \geq 50$  ps) EPW spectrum [Fig. 137.61(b)] is much broader than the linearly unstable spectrum. It is dominated by the common plasma waves (which are much greater in amplitude than before), while there are no obvious signatures of the cooperative absolute instability. It appears that a combination of profile modification and IAW turbulence excited by the nonlinear evolution of the absolutely unstable modes is able to restore growth to modes that were previously convectively saturated [Eq. (6)].<sup>19,169</sup> The turbulent restoration of temporal growth in parametric instabilities has been noted in the past.<sup>170–173</sup>

The broad EPW spectrum predicted by the extended Zakharov model in the nonlinear saturated state is consistent with experimental observations of half-harmonic optical emission and Thomson-scattering spectra (**Optical Signatures of Multibeam TPD**, p. 71). Similar calculations to those shown in Fig. 137.61, where the electron distribution function is evolved in the quasilinear approximation, also see a broad emission angle for TPD-produced hot electrons.<sup>149</sup> In the quasilinear approximation, electron acceleration is a stochastic process. As described in **Angular Properties of Hot-Electron Production**

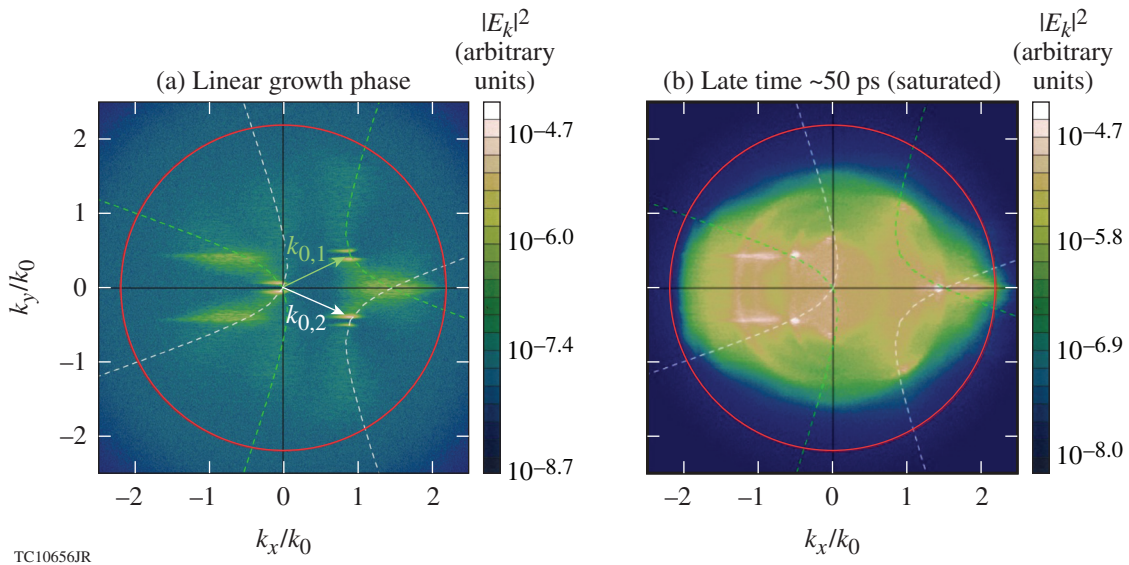


Figure 137.61 EPW spectra obtained from extended Zakharov calculations of TPD initiated by two crossing EM waves with wave vectors  $\vec{k}_{0,1}$  and  $\vec{k}_{0,2}$  (Refs. 19 and 169). The single-beam maximum growth-rate curves are shown for each (dashed hyperbolas) and the red circle is the Landau cutoff ( $|\vec{k}| \lambda_{De} = 0.25$ ). The spectrum at (a) early times ( $t = 6$  ps) and (b) late times ( $t \geq 50$  ps) when the instability has nonlinearly saturated (the simulation parameters are given in the text).

by **Multibeam TPD** (p. 71), a broad angular distribution of hot electrons is observed experimentally in multibeam interactions.

The computational efficiency of the quasilinear Zakharov model of TPD is such that 3-D calculations are quite practical to perform.<sup>132,169</sup> Since it is in only three dimensions that the full effects of multibeam interactions can be investigated, this approach holds much promise.

### Mitigation of Multibeam Instabilities

In general, despite the beneficial use of CBET in the indirect-drive-ignition campaign to control symmetry, it is preferable to avoid multibeam interactions wherever possible, i.e., mitigate their effects.

A few general principles apply to the mitigation of multibeam instabilities. If the instabilities are convective, and of the “induced” type (**Three-Wave Interactions**, p. 61), then for a given gain, the effect can be reduced by lowering the amplitude of the seed from which it grows. For CBET in indirect drive, this is not possible since the drive beams are themselves the seed. In direct drive, the seed is provided by unabsorbed light (**CBET in Direct Drive**, p. 64) that can be modified. This observation has led to concepts such as the use of smaller focal spots,<sup>89</sup> or focal-spot zooming, where the spot sizes are reduced during the main drive.<sup>174–177</sup>

The gain for convectively unstable multibeam instabilities involving low-frequency daughter waves (IAW’s) (i.e., CBET) may be reduced by modifying the frequencies of the interacting beams on existing laser systems, as demonstrated in indirect drive on the NIF (**CBET in Indirect Drive on the NIF**, p. 64). Direct-drive implosions require a larger  $\Delta\lambda$  among the beams to eliminate the resonant couplings relative to indirect drive because of the backscattering (compared with forward-scattering) geometry. Calculations performed by Igumenshchev *et al.*<sup>88,89</sup> indicate that frequency shifts of  $\Delta\lambda \gtrsim 5 \text{ \AA}$  (at  $3\omega_0$ ) can have a mitigating effect. Very large bandwidths are required to mitigate multibeam TPD,<sup>19</sup> but there is no fundamental reason why future laser systems cannot be constructed with this in mind.<sup>178</sup>

Multibeam gain can be reduced by increasing the plasma temperature (since gains are usually inversely proportional to the plasma temperature)<sup>3</sup> or by reducing the plasma density. This increase can be brought about by increasing absorption, through the use of higher- $Z$  hohlraum fill gases,<sup>179</sup> high- $Z$  ablators, or ablators with high- $Z$  layers.<sup>29,89,180</sup> Other more-exotic means, such as magnetizing thermal transport, may be

possible.<sup>181</sup> For multibeam instabilities that share decay waves (**Three-Wave Interactions**, p. 61), the above observations still hold, except it may be possible to additionally reduce the level of cooperation between beams by making suitable choices of beam pointing or by moving regions of high gain away from regions where the beams overlap.<sup>37</sup>

For instabilities that are not expected to be in the linearly convective regime, nonlinear models can provide insight into possible mitigation strategies. Figure 137.62 shows the results from 2-D quasilinear Zakharov calculations of TPD.<sup>149</sup> It can be seen that hot-electron production differs between plasmas of different effective ionization states for the same plasma parameters ( $L_n = 330 \mu\text{m}$ ,  $T_e = 2 \text{ keV}$ ). In these calculations,<sup>149</sup> the TPD was driven by two overlapping EM waves (as in Fig. 137.61). There are two contributing effects: The higher- $Z$  plasma has a higher collisional damping rate  $\nu_e$  for EPW’s, which modifies both the linear threshold and the nonlinear saturation.<sup>149</sup> Similar effects of EPW collisional damping on nonlinear saturation and hot-electron production were observed in PIC calculations

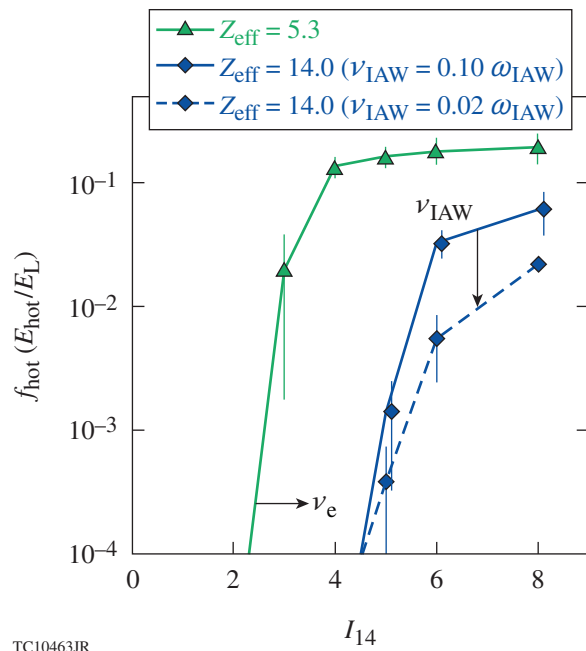


Figure 137.62

The simulated hot-electron fraction (energy in hot electrons normalized by laser energy) generated by TPD for three materials is shown as a function of overlapped laser intensity (in units of  $1 \times 10^{14} \text{ W/cm}^2$ ). The green curve corresponds to a CH plasma with  $Z_{\text{eff}} = 5.3$  and a normalized ion-acoustic damping rate  $\nu_{\text{IAW}}/\omega_{\text{IAW}} = 0.1$ . The blue solid (dashed) curves correspond to a material of higher effective  $Z$  ( $Z_{\text{eff}} = 14$ ) with  $\nu_{\text{IAW}}/\omega_{\text{IAW}} = 0.1$  ( $0.02$ ). In all cases,  $L_n = 330 \mu\text{m}$  and  $T_e = 2 \text{ keV}$ . These results have been taken from Ref. 149.

of TPD.<sup>159</sup> Lower hot-electron production in higher-Z ablators has been observed experimentally.<sup>182</sup> A reduction in the ion-acoustic damping rate  $\nu_{IAW}$  is shown to lead to a reduction in hot-electron production. This is a nonlinear effect that arises because of the role played by IAW's in the saturation of TPD.<sup>149</sup> Note that a similar effect has been observed experimentally for SRS in the small  $k\lambda_{De}$  regime.<sup>64,183</sup>

In practice, it might be necessary to use some combination of all of these effects to limit the deleterious effects of multi-beam interactions.

### Summary and Discussion

A description of both the direct- and indirect-drive approaches to ICF has been presented, with an emphasis placed on the differences in conditions between the two and the resulting impact on laser-plasma instabilities involving multiple beams. The ability of different laser beams to become cooperatively unstable has been discussed in the context of three-wave interactions.

This article has reviewed the experimental evidence for three-wave multibeam LPI's of relevance to laser-driven inertial confinement fusion at the ignition scale. The instabilities described are cross-beam energy transfer, multibeam stimulated Raman scattering, and multibeam two-plasmon decay. Cross-beam energy transfer is seen to be common to both ICF approaches, and the similarities and differences were described, together with the different routes taken to numerically compute the effect. Multibeam SRS appears to be unique to indirect drive, while TPD is of more importance to direct drive.

Calculations of multibeam SRS that involve sharing a common EM wave were presented. These *pF3D* calculations involved the combination of three different numerical codes and highlight one of the problems with LPI's in ICF—the scale mixing. The experimental evidence for multibeam TPD was discussed in some detail since it has recently become a very active area of experimental research. Similarly, advances in the theoretical understanding (both linear and nonlinear) were also presented. The linear theory of multibeam TPD was shown to be complicated by the presence of absolute instability, which necessitates the use of nonlinear models. The effect of nonlinearity on the EPW spectrum was shown, taking results from extended Zakharov models.

This article concluded with a discussion of the general principles by which multibeam instabilities can be either avoided or mitigated. The final implication is that LPI's in ICF should

be viewed from a description based on multibeam rather than single-beam concepts.

### ACKNOWLEDGMENT

The authors are grateful for the contributions from H. X. Vu (University of California, San Diego) and D. A. Russell and D. F. Dubois (Lodestar Research Corporation). This material is based upon work supported by the Department of Energy National Nuclear Security Administration under Award Number DE-NA0001944, the University of Rochester, and the New York State Energy Research and Development Authority. The support of DOE does not constitute an endorsement by DOE of the views expressed in this article.

### REFERENCES

1. J. Nuckolls *et al.*, *Nature* **239**, 139 (1972).
2. J. D. Lindl, *Inertial Confinement Fusion: The Quest for Ignition and Energy Gain Using Indirect Drive* (Springer-Verlag, New York, 1998).
3. W. L. Kruer, in *The Physics of Laser Plasma Interactions*, *Frontiers in Physics*, Vol. 73, edited by D. Pines (Addison-Wesley, Redwood City, CA, 1988).
4. S. H. Glenzer *et al.*, *Science* **327**, 1228 (2010).
5. P. A. Norreys, *Science* **327**, 1208 (2010).
6. R. L. McCrory, R. Betti, T. R. Boehly, D. T. Casey, T. J. B. Collins, R. S. Craxton, J. A. Delettrez, D. H. Edgell, R. Epstein, J. A. Frenje, D. H. Froula, M. Gatu-Johnson, V. Yu. Glebov, V. N. Goncharov, D. R. Harding, M. Hohenberger, S. X. Hu, I. V. Igumenshchev, T. J. Kessler, J. P. Knauer, C. K. Li, J. A. Marozas, F. J. Marshall, P. W. McKenty, D. D. Meyerhofer, D. T. Michel, J. F. Myatt, P. M. Nilson, S. J. Padalino, R. D. Petrasso, P. B. Radha, S. P. Regan, T. C. Sangster, F. H. Séguin, W. Seka, R. W. Short, A. Shvydky, S. Skupsky, J. M. Soures, C. Stoeckl, W. Theobald, B. Yaakobi, and J. D. Zuegel, *Nucl. Fusion* **53**, 113021 (2013).
7. J. D. Lindl *et al.*, *Phys. Plasmas* **11**, 339 (2004).
8. G. B. Zimmerman and W. L. Kruer, *Comments Plasma Phys. Control. Fusion* **2**, 51 (1975).
9. P. B. Radha, T. J. B. Collins, J. A. Delettrez, Y. Elbaz, R. Epstein, V. Yu. Glebov, V. N. Goncharov, R. L. Keck, J. P. Knauer, J. A. Marozas, F. J. Marshall, R. L. McCrory, P. W. McKenty, D. D. Meyerhofer, S. P. Regan, T. C. Sangster, W. Seka, D. Shvarts, S. Skupsky, Y. Srebro, and C. Stoeckl, *Phys. Plasmas* **12**, 056307 (2005).
10. D. H. Froula, D. T. Michel, I. V. Igumenshchev, S. X. Hu, B. Yaakobi, J. F. Myatt, D. H. Edgell, R. Follett, V. Yu. Glebov, V. N. Goncharov, T. J. Kessler, A. V. Maximov, P. B. Radha, T. C. Sangster, W. Seka, R. W. Short, A. A. Solodov, C. Sorce, and C. Stoeckl, *Plasma Phys. Control. Fusion* **54**, 124016 (2012).
11. J. D. Moody *et al.*, *Nat. Phys.* **8**, 344 (2012).
12. J. M. Dawson, *Rev. Mod. Phys.* **55**, 403 (1983).
13. C. K. Birdsall and A. B. Langdon, *Plasma Physics via Computer Simulation* (McGraw-Hill, New York, 1985).

14. R. A. Fonseca *et al.*, *Lect. Notes Comput. Sci.* **2331**, 342 (2002).
15. K. J. Bowers *et al.*, *Phys. Plasmas* **15**, 055703 (2008); K. L. Bowers *et al.*, in the *Proceedings of the 2008 ACM/IEEE Conference on Supercomputing* (IEEE Press, Piscataway, NJ, 2008); K. J. Bowers *et al.*, *J. Phys.: Conf. Ser.* **180**, 012055 (2009).
16. D. Pesme, S. Hüller, J. Myatt, C. Riconda, A. Maximov, V. T. Tikhonchuk, C. Labaune, J. Fuchs, S. Depierreux, and H. A. Baldis, *Plasma Phys. Control. Fusion* **44**, B53 (2002).
17. R. L. Berger *et al.*, *Phys. Plasmas* **5**, 4337 (1998); C. H. Still *et al.*, *Phys. Plasmas* **7**, 2023 (2000).
18. S. Hüller *et al.*, *Phys. Plasmas* **13**, 022703 (2006).
19. J. Zhang, J. F. Myatt, R. W. Short, A. V. Maximov, H. X. Vu, D. F. DuBois, and D. A. Russell, "Multibeam Two-Plasmon Decay from Linear Threshold to Nonlinear Saturations," to be published in *Physical Review Letters*.
20. H. X. Vu, D. F. DuBois, D. A. Russell, J. F. Myatt, and J. Zhang, "Non-linear Development of the Two-Plasmon-Decay Instability in Three Dimensions," submitted to *Physics of Plasmas*.
21. J. D. Lindl, *Phys. Plasmas* **2**, 3933 (1995).
22. M. J. Edwards, P. K. Patel, J. D. Lindl, L. J. Atherton, S. H. Glenzer, S. W. Haan, J. D. Kilkenny, O. L. Landen, E. I. Moses, A. Nikroo, R. Petrasso, T. C. Sangster, P. T. Springer, S. Batha, R. Benedetti, L. Bernstein, R. Betti, D. L. Bleuel, T. R. Boehly, D. K. Bradley, J. A. Caggiano, D. A. Callahan, P. M. Celliers, C. J. Cerjan, K. C. Chen, D. S. Clark, G. W. Collins, E. L. Dewald, L. Divol, S. Dixit, T. Doeppner, D. H. Edgell, J. E. Fair, M. Farrell, R. J. Fortner, J. Frenje, M. G. Gatu Johnson, E. Giraldez, V. Yu. Glebov, G. Grim, B. A. Hammel, A. V. Hamza, D. R. Harding, S. P. Hatchett, N. Hein, H. W. Herrmann, D. Hicks, D. E. Hinkel, M. Hoppe, W. W. Hsing, N. Izumi, B. Jacoby, O. S. Jones, D. Kalantar, R. Kauffman, J. L. Kline, J. P. Knauer, J. A. Koch, B. J. Koziolowski, G. Kyrala, K. N. LaFortune, S. Le Pape, R. J. Leeper, R. Lerche, T. Ma, B. J. MacGowan, A. J. MacKinnon, A. Macphee, E. R. Mapoles, M. M. Marinak, M. Mauldin, P. W. McKenty, M. Meezan, P. A. Michel, J. Milovich, J. D. Moody, M. Moran, D. H. Munro, C. L. Olson, K. Opachich, A. E. Pak, T. Parham, H.-S. Park, J. E. Ralph, S. P. Regan, B. Remington, H. Rinderknecht, H. F. Robey, M. Rosen, S. Ross, J. D. Salmonson, J. Sater, D. H. Schneider, F. H. Séguin, S. M. Sepke, D. A. Shaughnessy, V. A. Smalyuk, B. K. Spears, C. Stoeckl, W. Stoeffl, L. Suter, C. A. Thomas, R. Tommasini, R. P. Town, S. V. Weber, P. J. Wegner, K. Widman, M. Wilke, D. C. Wilson, C. B. Yeamans, and A. Zylstra, *Phys. Plasmas* **20**, 070501 (2013).
23. S. W. Haan, J. D. Lindl, D. A. Callahan, D. S. Clark, J. D. Salmonson, B. A. Hammel, L. J. Atherton, R. C. Cook, M. J. Edwards, S. Glenzer, A. V. Hamza, S. P. Hatchett, M. C. Herrmann, D. E. Hinkel, D. D. Ho, H. Huang, O. S. Jones, J. Kline, G. Kyrala, O. L. Landen, B. J. MacGowan, M. M. Marinak, D. D. Meyerhofer, J. L. Milovich, K. A. Moreno, E. I. Moses, D. H. Munro, A. Nikroo, R. E. Olson, K. Peterson, S. M. Pollaine, J. E. Ralph, H. F. Robey, B. K. Spears, P. T. Springer, L. J. Suter, C. A. Thomas, R. P. Town, R. Vesey, S. V. Weber, H. L. Wilkens, and D. C. Wilson, *Phys. Plasmas* **18**, 051001 (2011); M. J. Edwards, J. D. Lindl, B. K. Spears, S. V. Weber, L. J. Atherton, D. L. Bleuel, D. K. Bradley, D. A. Callahan, C. J. Cerjan, D. Clark, G. W. Collins, J. E. Fair, R. J. Fortner, S. H. Glenzer, S. W. Haan, B. A. Hammel, A. V. Hamza, S. P. Hatchett, N. Izumi, B. Jacoby, O. S. Jones, J. A. Koch, B. J. Koziolowski, O. L. Landen, R. Lerche, B. J. MacGowan, A. J. MacKinnon, E. R. Mapoles, M. M. Marinak, M. Moran, E. I. Moses, D. H. Munro, D. H. Schneider, S. M. Sepke, D. A. Shaughnessy, P. T. Springer, R. Tommasini, L. Bernstein, W. Stoeffl, R. Betti, T. R. Boehly, T. C. Sangster, V. Yu. Glebov, P. W. McKenty, S. P. Regan, D. H. Edgell, J. P. Knauer, C. Stoeckl, D. R. Harding, S. Batha, G. Grim, H. W. Herrmann, G. Kyrala, M. Wilke, D. C. Wilson, J. Frenje, R. Petrasso, K. Moreno, H. Huang, K. C. Chen, E. Giraldez, J. D. Kilkenny, M. Mauldin, N. Hein, M. Hoppe, A. Nikroo, and R. J. Leeper, *Phys. Plasmas* **18**, 051003 (2011); O. L. Landen, J. Edwards, S. W. Haan, H. F. Robey, J. Milovich, B. K. Spears, S. V. Weber, D. S. Clark, J. D. Lindl, B. J. MacGowan, E. I. Moses, J. Atherton, P. A. Amendt, T. R. Boehly, D. K. Bradley, D. G. Braun, D. A. Callahan, P. M. Celliers, G. W. Collins, E. L. Dewald, L. Divol, J. A. Frenje, S. H. Glenzer, A. Hamza, B. A. Hammel, D. G. Hicks, N. Hoffman, N. Izumi, O. S. Jones, J. D. Kilkenny, R. K. Kirkwood, J. L. Kline, G. A. Kyrala, M. M. Marinak, N. Meezan, D. D. Meyerhofer, P. Michel, D. H. Munro, R. E. Olson, A. Nikroo, S. P. Regan, L. J. Suter, C. A. Thomas, and D. C. Wilson, *Phys. Plasmas* **18**, 051002 (2011).
24. E. I. Moses *et al.*, *Phys. Plasmas* **16**, 041006 (2009); E. I. Moses, *Fusion Sci. Technol.* **54**, 361 (2008); W. J. Hogan, E. I. Moses, B. E. Warner, M. S. Sorem, and J. M. Soures, *Nucl. Fusion* **41**, 567 (2001); J. A. Paisner, E. M. Campbell, and W. J. Hogan, *Fusion Technol.* **26**, 755 (1994).
25. S. Skupsky, J. A. Marozas, R. S. Craxton, R. Betti, T. J. B. Collins, J. A. Delettrez, V. N. Goncharov, P. W. McKenty, P. B. Radha, T. R. Boehly, J. P. Knauer, F. J. Marshall, D. R. Harding, J. D. Kilkenny, D. D. Meyerhofer, T. C. Sangster, and R. L. McCrory, *Phys. Plasmas* **11**, 2763 (2004).
26. T. R. Boehly, D. L. Brown, R. S. Craxton, R. L. Keck, J. P. Knauer, J. H. Kelly, T. J. Kessler, S. A. Kumpan, S. J. Loucks, S. A. Letzring, F. J. Marshall, R. L. McCrory, S. F. B. Morse, W. Seka, J. M. Soures, and C. P. Verdon, *Opt. Commun.* **133**, 495 (1997).
27. L. J. Waxer, D. N. Maywar, J. H. Kelly, T. J. Kessler, B. E. Kruschwitz, S. J. Loucks, R. L. McCrory, D. D. Meyerhofer, S. F. B. Morse, C. Stoeckl, and J. D. Zuegel, *Opt. Photonics News* **16**, 30 (2005).
28. D. N. Maywar, J. H. Kelly, L. J. Waxer, S. F. B. Morse, I. A. Begishev, J. Bromage, C. Dorner, J. L. Edwards, L. Folsbee, M. J. Guardalben, S. D. Jacobs, R. Jungquist, T. J. Kessler, R. W. Kidder, B. E. Kruschwitz, S. J. Loucks, J. R. Marcianti, R. L. McCrory, D. D. Meyerhofer, A. V. Okishev, J. B. Oliver, G. Pien, J. Qiao, J. Puth, A. L. Rigatti, A. W. Schmid, M. J. Shoup III, C. Stoeckl, K. A. Thorp, and J. D. Zuegel, *J. Phys., Conf. Ser.* **112**, 032007 (2008).
29. V. N. Goncharov, T. C. Sangster, R. Betti, T. R. Boehly, T. J. B. Collins, R. S. Craxton, J. A. Delettrez, D. H. Edgell, R. Epstein, R. Follet, C. J. Forrest, D. H. Froula, V. Y. Glebov, D. R. Harding, R. Henchen, S. X. Hu, I. V. Igumenshchev, R. Janezic, J. H. Kelly, T. J. Kessler, T. Z. Kosc, S. J. Loucks, J. A. Marozas, F. J. Marshall, A. V. Maximov, R. L. McCrory, P. W. McKenty, D. D. Meyerhofer, D. T. Michel, J. F. Myatt, R. Nora, P. B. Radha, S. P. Regan, W. Seka, W. T. Shmayda, R. W. Short, A. Shvydky, S. Skupsky, C. Stoeckl, B. Yaakobi, J. A. Frenje, M. Gatu-Johnson, R. D. Petrasso, and D. T. Casey, "Improving the Hot-Spot Pressure and Demonstrating Ignition Hydrodynamic Equivalence in Cryogenic DT Implosions on OMEGA," to be published in *Physics of Plasmas*.

30. T. J. B. Collins, J. A. Marozas, and P. W. McKenty, *Bull. Am. Phys. Soc.* **57**, 155 (2012); T. J. B. Collins, J. A. Marozas, K. S. Anderson, R. Betti, R. S. Craxton, J. A. Delettrez, V. N. Goncharov, D. R. Harding, F. J. Marshall, R. L. McCrory, D. D. Meyerhofer, P. W. McKenty, P. B. Radha, A. Shvydky, S. Skupsky, and J. D. Zuegel, *Phys. Plasmas* **19**, 056308 (2012).
31. S. W. Haan *et al.*, *Phys. Plasmas* **2**, 2480 (1995).
32. P. Michel *et al.*, *Phys. Rev. E* **83**, 046409 (2011).
33. R. L. McCrory, D. D. Meyerhofer, R. Betti, R. S. Craxton, J. A. Delettrez, D. H. Edgell, V. Yu Glebov, V. N. Goncharov, D. R. Harding, D. W. Jacobs-Perkins, J. P. Knauer, F. J. Marshall, P. W. McKenty, P. B. Radha, S. P. Regan, T. C. Sangster, W. Seka, R. W. Short, S. Skupsky, V. A. Smalyuk, J. M. Soures, C. Stoeckl, B. Yaakobi, D. Shvarts, J. A. Frenje, C. K. Li, R. D. Petrasso, and F. H. Séguin, *Phys. Plasmas* **15**, 055503 (2008).
34. E. A. Williams, B. I. Cohen, L. Divol, M. R. Dorr, J. A. Hittinger, D. E. Hinkel, A. B. Langdon, R. K. Kirkwood, D. H. Froula, and S. H. Glenzer, *Phys. Plasmas* **11**, 231 (2004).
35. D. J. Strozzi, E. A. Williams, D. E. Hinkel, D. H. Froula, R. A. London, and D. A. Callahan, *Phys. Plasmas* **15**, 102703 (2008).
36. S. Laffite and P. Loiseau, *Phys. Plasmas* **17**, 102704 (2010).
37. D. E. Hinkel *et al.*, *Phys. Plasmas* **18**, 056312 (2011).
38. H. Motz, *The Physics of Laser Fusion* (Academic Press, London, 1979).
39. R. C. Davidson, *Methods in Nonlinear Plasma Theory* (Academic Press, New York, 1972).
40. D. Pesme, in *L'Interaction Laser-Matière, Part I*, edited by L. Bergé *et al.*, La Fusion Thermonucléaire Inertielle par Laser, Collection du Commissariat à l'énergie Atomique, edited by R. Dautray and J.-P. Wateau (Eyrolles, Paris, 1993), Vol. 1, Chap. 2, Sec. IV.3, pp. 306–350.
41. R. J. Briggs, *Electron-Stream Interaction with Plasmas* (MIT Press, Cambridge, MA, 1964).
42. A. Bers, in *Physique des Plasmas: Université de Grenoble, Summer School of Theoretical Physics, Les Houches 1972*, edited by C. DeWitt and J. Peyraud (Gordon and Breach, New York, 1975).
43. M. N. Rosenbluth, *Phys. Rev. Lett.* **29**, 565 (1972).
44. D. F. DuBois, B. Bezzerides, and H. A. Rose, *Phys. Fluids B* **4**, 241 (1992).
45. W. L. Kruer *et al.*, *Phys. Plasmas* **3**, 382 (1996).
46. R. K. Kirkwood, P. Michel, R. London, J. D. Moody, E. Dewald, L. Yin, J. Kline, D. Hinkel, D. Callahan, N. Meezan, E. Williams, L. Divol, B. L. Albright, K. J. Bowers, E. Bond, H. Rose, Y. Ping, T. L. Wang, C. Joshi, W. Seka, N. J. Fisch, D. Turnbull, S. Suckewer, J. S. Wurtele, S. Glenzer, L. Suter, C. Haynam, O. Landen, and B. J. Macgowan, *Phys. Plasmas* **18**, 056311 (2011).
47. H. A. Rose and D. F. DuBois, *Phys. Fluids B* **4**, 252 (1992).
48. J. S. Li *et al.*, *Bull. Am. Phys. Soc.* **39**, 1584 (1994).
49. H. A. Rose, *Phys. Plasmas* **3**, 1709 (1996).
50. D. E. Hinkel, E. A. Williams, and C. H. Still, *Phys. Rev. Lett.* **77**, 1298 (1996).
51. J. D. Moody *et al.*, *Phys. Rev. Lett.* **77**, 1294 (1996).
52. N. M. Kroll, A. Ron, and N. Rostoker, *Phys. Rev. Lett.* **13**, 83 (1964); B. L. Stansfield, R. Nodwell, and J. Meyer, *Phys. Rev. Lett.* **26**, 1219 (1971).
53. C. J. Pawley, H. E. Huey, and N. C. Luhmann, Jr., *Phys. Rev. Lett.* **49**, 877 (1982); C. W. Domier and N. C. Luhmann, Jr., *Phys. Rev. Lett.* **69**, 3499 (1992); D. M. Villeneuve, H. A. Baldis, and J. E. Bernard, *Phys. Rev. Lett.* **59**, 1585 (1987).
54. E. A. Williams, D. M. Lininger, and M. V. Goldman, *Phys. Fluids B* **1**, 1561 (1989).
55. V. M. Malkin, G. Shvets, and N. J. Fisch, *Phys. Rev. Lett.* **82**, 4448 (1999); Y. Ping *et al.*, *Phys. Plasmas* **16**, 123113 (2009).
56. R. M. G. M. Trines *et al.*, *Nat. Phys.* **7**, 87 (2010).
57. D. S. Clark and N. J. Fisch, *Phys. Plasmas* **10**, 3363 (2003).
58. R. K. Kirkwood *et al.*, *Plasma Phys. Control. Fusion* **55**, 103001 (2013).
59. V. V. Eliseev *et al.*, *Phys. Plasmas* **3**, 2215 (1996).
60. C. J. McKinstrie *et al.*, *Phys. Plasmas* **3**, 2686 (1996).
61. H. A. Rose and S. Ghosal, *Phys. Plasmas* **5**, 1461 (1998).
62. B. I. Cohen *et al.*, *Phys. Plasmas* **5**, 3408 (1998).
63. J. A. F. Hittinger *et al.*, *J. Comput. Phys.* **209**, 695 (2005).
64. R. K. Kirkwood *et al.*, *Phys. Rev. Lett.* **77**, 2706 (1996).
65. H. A. Baldis *et al.*, *Phys. Rev. Lett.* **77**, 2957 (1996).
66. A. K. Lal *et al.*, *Phys. Rev. Lett.* **78**, 670 (1997).
67. J. C. Fernández *et al.*, *Phys. Rev. Lett.* **81**, 2252 (1998).
68. K. B. Wharton *et al.*, *Phys. Rev. Lett.* **81**, 2248 (1998).
69. K. B. Wharton *et al.*, *Phys. Plasmas* **6**, 2144 (1999).
70. C. Labaune *et al.*, *Phys. Plasmas* **6**, 2048 (1999).
71. C. Labaune *et al.*, *Phys. Rev. Lett.* **85**, 1658 (2000).
72. R. K. Kirkwood, J. D. Moody, A. B. Langdon, B. I. Cohen, E. A. Williams, M. R. Dorr, J. A. Hittinger, R. Berger, P. E. Young, L. J. Suter, L. Divol, S. H. Glenzer, O. L. Landen, and W. Seka, *Phys. Rev. Lett.* **89**, 215003 (2002).
73. R. K. Kirkwood *et al.*, *Phys. Rev. Lett.* **76**, 2065 (1996).
74. K. Marsh, C. Joshi, and C. McKinstrie, *Bull. Am. Phys. Soc.* **39**, 1585 (1994).

75. C. Labaune *et al.*, Phys. Rev. Lett. **82**, 3613 (1999).
76. P. Michel *et al.*, Phys. Rev. Lett. **102**, 025004 (2009).
77. P. Michel *et al.*, Phys. Plasmas **16**, 042702 (2009).
78. C. J. Randall, J. J. Thomson, and K. G. Estabrook, Phys. Rev. Lett. **43**, 924 (1979); C. J. Randall, J. R. Albritton, and J. J. Thomson, Phys. Fluids **24**, 1474 (1981).
79. W. Seka, H. A. Baldis, J. Fuchs, S. P. Regan, D. D. Meyerhofer, C. Stoeckl, B. Yaakobi, R. S. Craxton, and R. W. Short, Phys. Rev. Lett. **89**, 175002 (2002).
80. J. Myatt, A. V. Maximov, W. Seka, R. S. Craxton, and R. W. Short, Phys. Plasmas **11**, 3394 (2004).
81. A. V. Maximov, J. Myatt, W. Seka, R. W. Short, and R. S. Craxton, Phys. Plasmas **11**, 2994 (2004).
82. T. Dewandre, J. R. Albritton, and E. A. Williams, Phys. Fluids **24**, 528 (1981).
83. J. Delettrez, R. Epstein, M. C. Richardson, P. A. Jaanimagi, and B. L. Henke, Phys. Rev. A **36**, 3926 (1987).
84. D. H. Edgell, W. Seka, J. A. Delettrez, R. S. Craxton, V. N. Goncharov, I. V. Igumenshchev, J. Myatt, A. V. Maximov, R. W. Short, T. C. Sangster, and R. E. Bahr, Bull. Am. Phys. Soc. **52**, 195 (2007).
85. D. H. Edgell, W. Seka, J. A. Delettrez, R. S. Craxton, V. N. Goncharov, I. V. Igumenshchev, J. F. Myatt, A. V. Maximov, R. W. Short, T. C. Sangster, and R. E. Bahr, Bull. Am. Phys. Soc. **54**, 145 (2009).
86. D. H. Edgell, W. Seka, J. A. Delettrez, R. S. Craxton, V. N. Goncharov, I. V. Igumenshchev, J. F. Myatt, A. V. Maximov, R. W. Short, T. C. Sangster, and R. E. Bahr, Bull. Am. Phys. Soc. **53**, 168 (2008).
87. W. Seka, D. H. Edgell, J. P. Knauer, J. F. Myatt, A. V. Maximov, R. W. Short, T. C. Sangster, C. Stoeckl, R. E. Bahr, R. S. Craxton, J. A. Delettrez, V. N. Goncharov, I. V. Igumenshchev, and D. Shvarts, Phys. Plasmas **15**, 056312 (2008).
88. I. V. Igumenshchev, D. H. Edgell, V. N. Goncharov, J. A. Delettrez, A. V. Maximov, J. F. Myatt, W. Seka, A. Shvydky, S. Skupsky, and C. Stoeckl, Phys. Plasmas **17**, 122708 (2010).
89. I. V. Igumenshchev, W. Seka, D. H. Edgell, D. T. Michel, D. H. Froula, V. N. Goncharov, R. S. Craxton, L. Divol, R. Epstein, R. Follett, J. H. Kelly, T. Z. Kosc, A. V. Maximov, R. L. McCrory, D. D. Meyerhofer, P. Michel, J. F. Myatt, T. C. Sangster, A. Shvydky, S. Skupsky, and C. Stoeckl, Phys. Plasmas **19**, 056314 (2012).
90. I. V. Igumenshchev, D. H. Edgell, V. N. Goncharov, J. A. Delettrez, A. V. Maximov, J. F. Myatt, W. Seka, and A. Shvydky, Bull. Am. Phys. Soc. **54**, 145 (2009).
91. V. N. Goncharov, O. V. Gotchev, E. Vianello, T. R. Boehly, J. P. Knauer, P. W. McKenty, P. B. Radha, S. P. Regan, T. C. Sangster, S. Skupsky, V. A. Smalyuk, R. Betti, R. L. McCrory, D. D. Meyerhofer, and C. Cherfils-Clérouin, Phys. Plasmas **13**, 012702 (2006).
92. D. T. Michel, C. Sorce, R. Epstein, N. Whiting, I. V. Igumenshchev, R. Jungquist, and D. H. Froula, Rev. Sci. Instrum. **83**, 10E530 (2012).
93. D. H. Froula, I. V. Igumenshchev, D. T. Michel, D. H. Edgell, R. Follett, V. Yu. Glebov, V. N. Goncharov, J. Kwiatkowski, F. J. Marshall, P. B. Radha, W. Seka, C. Sorce, S. Stagnitto, C. Stoeckl, and T. C. Sangster, Phys. Rev. Lett. **108**, 125003 (2012).
94. G. A. Kyrala *et al.*, Phys. Plasmas **18**, 072703 (2011).
95. N. B. Meezan *et al.*, Phys. Plasmas **17**, 056304 (2010).
96. P. Michel *et al.*, Phys. Plasmas **17**, 056305 (2010).
97. M. M. Marinak *et al.*, Phys. Plasmas **8**, 2275 (2001).
98. P. Michel *et al.*, Phys. Rev. Lett. **109**, 195004 (2012).
99. P. Michel *et al.*, Phys. Plasmas **20**, 056308 (2013).
100. D. E. Hinkel, M. J. Edwards, P. A. Amendt, R. Benedetti, L. Berzak Hopkins, D. Bleuel, T. R. Boehly, D. K. Bradley, J. A. Caggiano, D. A. Callahan, P. M. Celliers, C. J. Cerjan, D. Clark, G. W. Collins, E. L. Dewald, T. R. Dittrich, L. Divol, S. N. Dixit, T. Doepfner, D. Edgell, J. Eggert, D. Farley, J. A. Frenje, V. Glebov, S. M. Glenn, S. W. Haan, A. Hamza, B. A. Hammel, C. A. Haynam, J. H. Hammer, R. F. Heeter, H. W. Herrmann, D. Ho, O. Hurricane, N. Izumi, M. Gatun Johnson, O. S. Jones, D. H. Kalantar, R. L. Kauffman, J. D. Kilkenny, J. L. Kline, J. P. Knauer, J. A. Koch, A. Kritcher, G. A. Kyrala, K. LaFortune, O. L. Landen, B. F. Lasinski, T. Ma, A. J. Mackinnon, A. J. Macphee, E. Mapoles, J. L. Milovich, J. D. Moody, D. Meeker, N. B. Meezan, P. Michel, A. S. Moore, D. H. Munro, A. Nikroo, R. E. Olson, K. Opachich, A. Pak, T. Parham, P. Patel, H.-S. Park, R. D. Petrasso, J. Ralph, S. P. Regan, B. A. Remington, H. G. Rinderknecht, H. F. Robey, M. D. Rosen, J. S. Ross, R. Rygg, J. D. Salmonson, T. C. Sangster, M. B. Schneider, V. Smalyuk, B. K. Spears, P. T. Springer, E. Storm, D. J. Strozzi, L. J. Suter, C. A. Thomas, R. P. J. Town, E. A. Williams, S. V. Weber, P. J. Wegner, D. C. Wilson, K. Widmann, C. Yeamans, A. Zylstra, J. D. Lindl, L. J. Atherton, W. W. Hsing, B. J. MacGowan, B. M. Van Wousterghem, and E. I. Moses, Plasma Phys. Control. Fusion **55**, 124015 (2013).
101. D. E. Hinkel, presented at the HEDP Summer School, Columbus, OH, 15–19 July 2013.
102. D. E. Hinkel *et al.*, Phys. Plasmas **15**, 056314 (2008).
103. D. H. Froula, Phys. Rev. Lett. **103**, 045006 (2009).
104. D. H. Froula, L. Divol, R. A. London, R. L. Berger, T. Döppner, N. B. Meezan, J. Ralph, J. S. Ross, L. J. Suter, and S. H. Glenzer, Phys. Plasmas **17**, 056302 (2010).
105. J. D. Moody *et al.*, Phys. Rev. Lett. **111**, 025001 (2013).
106. R. P. J. Town *et al.*, Phys. Plasmas **18**, 056302 (2011).
107. M. D. Rosen *et al.*, High Energy Density Phys. **7**, 180 (2011).
108. T. Chapman *et al.*, Phys. Rev. Lett. **108**, 145003 (2012).
109. L. Yin *et al.*, Phys. Rev. Lett. **108**, 245004 (2012).
110. L. Yin *et al.*, Phys. Plasmas **19**, 056304 (2012).
111. L. Yin *et al.*, Phys. Plasmas **20**, 012702 (2013).

112. S. P. Regan, N. B. Meezan, L. J. Suter, D. J. Strozzi, W. L. Kruer, D. Meeker, S. H. Glenzer, W. Seka, C. Stoeckl, V. Yu. Glebov, T. C. Sangster, D. D. Meyerhofer, R. L. McCrory, E. A. Williams, O. S. Jones, D. A. Callahan, M. D. Rosen, O. L. Landen, C. Sorce, and B. J. MacGowan, *Phys. Plasmas* **17**, 020703 (2010).
113. W. Seka, D. H. Edgell, J. F. Myatt, A. V. Maximov, R. W. Short, V. N. Goncharov, and H. A. Baldis, *Phys. Plasmas* **16**, 052701 (2009).
114. N. A. Ebrahim *et al.*, *Phys. Rev. Lett.* **45**, 1179 (1980).
115. H. A. Baldis and C. J. Walsh, *Phys. Rev. Lett.* **47**, 1658 (1981).
116. D. M. Villeneuve, R. L. Keck, B. B. Afeyan, W. Seka, and E. A. Williams, *Phys. Fluids* **27**, 721 (1984).
117. C. Rousseaux *et al.*, *Phys. Fluids B* **4**, 2589 (1992).
118. B. Yaakobi, P.-Y. Chang, A. A. Solodov, C. Stoeckl, D. H. Edgell, R. S. Craxton, S. X. Hu, J. F. Myatt, F. J. Marshall, W. Seka, and D. H. Froula, *Phys. Plasmas* **19**, 012704 (2012).
119. M. V. Goldman, *Ann. Phys.* **38**, 117 (1966).
120. Y. C. Lee and P. K. Kaw, *Phys. Rev. Lett.* **32**, 135 (1974).
121. V. P. Silin and A. N. Starodub, *Sov. Phys.-JETP* **39**, 82 (1974).
122. A. B. Langdon, B. F. Lasinski, and W. L. Kruer, *Phys. Rev. Lett.* **43**, 133 (1979).
123. A. Simon, R. W. Short, E. A. Williams, and T. Dewandre, *Phys. Fluids* **26**, 3107 (1983).
124. H. X. Vu, D. F. DuBois, D. A. Russell, and J. F. Myatt, *Phys. Plasmas* **17**, 072701 (2010).
125. C. S. Liu and M. N. Rosenbluth, *Phys. Fluids* **19**, 967 (1976).
126. B. B. Afeyan and E. A. Williams, *Phys. Rev. Lett.* **75**, 4218 (1995).
127. D. T. Michel, A. V. Maximov, R. W. Short, S. X. Hu, J. F. Myatt, W. Seka, A. A. Solodov, B. Yaakobi, and D. H. Froula, *Phys. Rev. Lett.* **109**, 155007 (2012).
128. R. Yan, A. V. Maximov, and C. Ren, *Phys. Plasmas* **17**, 052701 (2010).
129. C. S. Liu, in *Advances in Plasma Physics*, edited by A. Simon and W. B. Thompson (Wiley-Interscience, New York, 1976), Vol. 6, pp. 167–174.
130. D. F. DuBois, D. A. Russell, and H. A. Rose, *Phys. Rev. Lett.* **74**, 3983 (1995).
131. D. T. Michel, A. V. Maximov, R. W. Short, J. A. Delettrez, D. Edgell, S. X. Hu, I. V. Igumenshchev, J. F. Myatt, A. A. Solodov, C. Stoeckl, B. Yaakobi, and D. H. Froula, *Phys. Plasmas* **20**, 055703 (2013).
132. J. Zhang, J. F. Myatt, A. V. Maximov, R. W. Short, D. F. DuBois, D. A. Russell, and H. X. Vu, *Bull. Am. Phys. Soc.* **57**, 299 (2012).
133. R. W. Short, J. F. Myatt, and J. Zhang, *Bull. Am. Phys. Soc.* **58**, 27 (2013).
134. H. Derblom *et al.*, *J. Geophys. Res., A, Space Phys.* **94**, 10111 (1989).
135. D. W. Phillion *et al.*, *Phys. Rev. Lett.* **49**, 1405 (1982).
136. W. Seka, R. E. Bahr, R. W. Short, A. Simon, R. S. Craxton, D. S. Montgomery, and A. E. Rubenchik, *Phys. Fluids B* **4**, 2232 (1992).
137. D. A. Russell and D. F. DuBois, *Phys. Rev. Lett.* **86**, 428 (2001).
138. R. E. Turner *et al.*, *Phys. Fluids* **27**, 511 (1984).
139. J. Meyer and Y. Zhu, *Phys. Rev. Lett.* **71**, 2915 (1993).
140. R. L. Berger and L. V. Powers, *Phys. Fluids* **28**, 2895 (1985).
141. L. V. Powers and R. J. Schroeder, *Phys. Rev. A* **29**, 2298 (1984).
142. A. N. Starodub and M. V. Filippov, *Sov. J. Plasma Phys.* **5**, 610 (1979).
143. V. Yu. Bychenkov, V. P. Silin, and V. T. Tikhonchuk, *Sov. J. Plasma Phys.* **3**, 730 (1977).
144. A. I. Avrov *et al.*, *Sov. Phys.-JETP* **45**, 507 (1977).
145. R. L. Keck, L. M. Goldman, M. C. Richardson, W. Seka, and K. Tanaka, *Phys. Fluids* **27**, 2762 (1984).
146. B. Yaakobi, I. Pelah, and J. Hoose, *Phys. Rev. Lett.* **37**, 836 (1976).
147. J. D. Hares *et al.*, *Phys. Rev. Lett.* **42**, 1216 (1979).
148. C. Stoeckl, R. E. Bahr, B. Yaakobi, W. Seka, S. P. Regan, R. S. Craxton, J. A. Delettrez, R. W. Short, J. Myatt, A. V. Maximov, and H. Baldis, *Phys. Rev. Lett.* **90**, 235002 (2003).
149. J. F. Myatt, H. X. Vu, D. F. DuBois, D. A. Russell, J. Zhang, R. W. Short, and A. V. Maximov, *Phys. Plasmas* **20**, 052705 (2013).
150. D. H. Froula, B. Yaakobi, S. X. Hu, P.-Y. Chang, R. S. Craxton, D. H. Edgell, R. Follett, D. T. Michel, J. F. Myatt, W. Seka, R. W. Short, A. Solodov, and C. Stoeckl, *Phys. Rev. Lett.* **108**, 165003 (2012).
151. W. Seka, D. H. Edgell, D. H. Froula, J. Katz, J. F. Myatt, J. Zhang, R. W. Short, D. T. Michel, A. V. Maximov, and V. N. Goncharov, *Bull. Am. Phys. Soc.* **57**, 299 (2012).
152. J. J. Schuss, T. K. Chu, and L. C. Johnson, *Phys. Rev. Lett.* **40**, 27 (1978).
153. H. A. Baldis, J. C. Samson, and P. B. Corkum, *Phys. Rev. Lett.* **41**, 1719 (1978).
154. R. K. Follett, D. T. Michel, S. X. Hu, J. F. Myatt, R. J. Henchen, J. Katz, and D. H. Froula, *Bull. Am. Phys. Soc.* **58**, 27 (2013).
155. V. N. Goncharov, T. C. Sangster, T. R. Boehly, S. X. Hu, I. V. Igumenshchev, F. J. Marshall, R. L. McCrory, D. D. Meyerhofer, P. B. Radha, W. Seka, S. Skupsky, C. Stoeckl, D. T. Casey, J. A. Frenje, and R. D. Petrasso, *Phys. Rev. Lett.* **104**, 165001 (2010).
156. J. F. Myatt, J. Zhang, J. A. Delettrez, A. V. Maximov, R. W. Short, W. Seka, D. H. Edgell, D. F. DuBois, D. A. Russell, and H. X. Vu, *Phys. Plasmas* **19**, 022707 (2012).
157. B. Yaakobi, A. A. Solodov, J. F. Myatt, J. A. Delettrez, C. Stoeckl, and D. H. Froula, *Phys. Plasmas* **20**, 092706 (2013).

158. R. Yan, A. V. Maximov, C. Ren, and F. S. Tsung, *Phys. Rev. Lett.* **103**, 175002 (2009).
159. R. Yan, C. Ren, J. Li, A. V. Maximov, W. B. Mori, Z.-M. Sheng, and F. S. Tsung, *Phys. Rev. Lett.* **108**, 175002 (2012).
160. C. Riconda *et al.*, *Phys. Plasmas* **18**, 092701 (2011).
161. S. Weber *et al.*, *Phys. Rev. E* **85**, 016403 (2012).
162. H. X. Vu, D. F. DuBois, J. F. Myatt, and D. A. Russell, *Phys. Plasmas* **19**, 102703 (2012).
163. H. X. Vu, D. F. DuBois, D. A. Russell, and J. F. Myatt, *Phys. Plasmas* **19**, 102708 (2012).
164. F. S. Tsung *et al.*, *Bull. Am. Phys. Soc.* **45**, 357 (2000); F. S. Tsung, B. B. Afeyan, and W. B. Mori, *Bull. Am. Phys. Soc.* **46**, 282 (2001); *ibid.* **48**, 45 (2003); *ibid.* **49**, 277 (2004); *ibid.* **50**, 120 (2005); *ibid.* **51**, 288 (2006); *ibid.* **52**, 43 (2007); *ibid.* **53**, 232 (2008); *ibid.* **54**, 210 (2009); *ibid.* **55**, 232 (2010); *ibid.* **56**, 329 (2011); *ibid.* **57**, 99 (2012).
165. P. A. Robinson, *Rev. Mod. Phys.* **69**, 507 (1997).
166. M. V. Goldman, *Rev. Mod. Phys.* **56**, 709 (1984).
167. D. A. Russell, D. F. DuBois, and H. X. Vu, presented at the Workshop on the Nonlinear Saturation of Stimulated Raman and Brillouin Instabilities for Plasma and Laser Parameters of Interest to Inertial Fusion Confinement and High Energy Density Science, Livermore, CA, 3–5 April 2002.
168. K. Y. Sanbonmatsu *et al.*, *Phys. Plasmas* **7**, 2824 (2000).
169. J. Zhang, J. F. Myatt, A. V. Maximov, R. W. Short, D. F. DuBois, D. A. Russell, and H. X. Vu, *Bull. Am. Phys. Soc.* **58**, 27 (2013).
170. E. Z. Gusakov, *Sov. J. Plasma Phys.* **8**, 324 (1982).
171. E. A. Williams, J. R. Albritton, and M. N. Rosenbluth, *Phys. Fluids* **22**, 139 (1979).
172. G. Laval, R. Pellat, and D. Pesme, *Phys. Rev. Lett.* **36**, 192 (1976).
173. D. R. Nicholson and A. N. Kaufman, *Phys. Rev. Lett.* **33**, 1207 (1974).
174. P. W. McKenty, R. S. Craxton, A. Shvydky, F. J. Marshall, J. A. Marozas, S. Skupsky, D. D. Meyerhofer, and R. L. McCrory, *Bull. Am. Phys. Soc.* **56**, 241 (2011).
175. I. V. Igumenshchev, D. H. Froula, D. H. Edgell, V. N. Goncharov, T. J. Kessler, F. J. Marshall, R. L. McCrory, P. W. McKenty, D. D. Meyerhofer, D. T. Michel, T. C. Sangster, W. Seka, and S. Skupsky, *Phys. Rev. Lett.* **110**, 145001 (2013).
176. P. Michel, *Physics* **6**, 37 (2013).
177. D. H. Froula, T. J. Kessler, I. V. Igumenshchev, R. Betti, V. N. Goncharov, H. Huang, S. X. Hu, E. Hill, J. H. Kelly, D. D. Meyerhofer, A. Shvydky, and J. D. Zuegel, *Phys. Plasmas* **20**, 082704 (2013).
178. D. Eimerl, E. M. Campbell, W. F. Krupke, J. Zweiback, W. L. Kruer, J. Zuegel, J. Myatt, J. Kelly, D. Froula, and R. L. McCrory, “StarDriver: A Flexible Laser Driver for Inertial Confinement Fusion and High Energy Density Physics,” submitted to the *Journal of Fusion Energy*.
179. D. J. Strozzi *et al.*, *Bull. Am. Phys. Soc.* **58**, 324 (2013).
180. M. Lafon, R. Betti, R. Nora, K. S. Anderson, T. J. B. Collins, and P. W. McKenty, *Bull. Am. Phys. Soc.* **58**, 324 (2013).
181. D. S. Montgomery, B. J. Albright, J. L. Kline, L. Yin, P. Y. Chang, J. R. Davies, G. Fiksel, D. H. Froula, R. Betti, and M. J. MacDonald, *Bull. Am. Phys. Soc.* **58**, 27 (2013).
182. V. A. Smalyuk, R. Betti, J. A. Delettrez, V. Yu. Glebov, D. D. Meyerhofer, P. B. Radha, S. P. Regan, T. C. Sangster, J. Sanz, W. Seka, C. Stoeckl, B. Yaakobi, J. A. Frenje, C. K. Li, R. D. Petrasso, and F. H. Séguin, *Phys. Rev. Lett.* **104**, 165002 (2010).
183. J. C. Fernández *et al.*, *Phys. Rev. Lett.* **77**, 2702 (1996).